JOURNAL OF GEOPHYSICAL RESEARCH, VOL. 113, B08S10, doi:10.1029/2007JB005215, 2008

Direct video and hydrophone observations of submarine explosive eruptions at NW Rota-1 volcano, Mariana arc

W. W. Chadwick Jr.,[1] K. V. Cashman,[2] R. W. Embley,[3] H. Matsumoto,[1] R. P. Dziak,[1] C. E. J. de Ronde,[4] T. K. Lau,[1] N. D. Deardorff,[2] and S. G. Merle[1]

Received 5 June 2007; revised 2 January 2008; accepted 1 February 2008; published 3 June 2008.

[1] Extraordinary video and hydrophone observations of a submarine explosive eruption were made with a remotely operated vehicle in April 2006 at a depth of 550–560 m on NW Rota-1 volcano in the Mariana arc. The observed eruption evolved from effusive to explosive, while the eruption rate increased from near zero to 10–100 m^3/h. During the peak in activity, cyclic explosive bursts 2–6 min long were separated by shorter non-eruptive pauses lasting 10–100 s. The size of the ejecta increased with the vigor of the explosions. A portable hydrophone deployed near the vent recorded sounds correlated with the explosive bursts; the highest amplitudes were ~50 dB higher than ambient noise at frequencies between 10 and 50 Hz. The acoustic data allow us to quantify the durations, amplitudes, and evolution of the eruptive events over time. The low eruption rate, high gas/lava ratio, and rhythmic eruptive behavior at NW Rota-1 are most consistent with a Strombolian eruptive style. We interpret that the eruption was primarily driven by the venting of magmatic gases, which was also the primary source of the sound recorded during the explosive bursts. The rhythmic nature of the bursts can be explained by partial gas segregation in the conduit and upward migration in a transitional regime between bubbly flow and fully developed slug flow. The strongest explosive bursts were accompanied by flashes of red glow and oscillating eruption plumes in the vent, apparently caused by magma-seawater interaction and rapid steam formation and condensation. This is the first time submarine explosive eruptions have been witnessed with simultaneous near-field acoustic recordings.

Citation: Chadwick, W. W., Jr., K. V. Cashman, R. W. Embley, H. Matsumoto, R. P. Dziak, C. E. J. de Ronde, T. K. Lau, N. D. Deardorff, and S. G. Merle (2008), Direct video and hydrophone observations of submarine explosive eruptions at NW Rota-1 volcano, Mariana arc, *J. Geophys. Res.*, *113*, B08S10, doi:10.1029/2007JB005215.

1. Introduction

[2] NW Rota-1 submarine volcano is located within the Mariana arc, an intraoceanic subduction zone where underwater volcanoes outnumber their subaerial counterparts by more than five times [*Bloomer et al.*, 1989; *Stern et al.*, 2003; *Embley et al.*, 2004]. NW Rota-1 is located at 14°36.0′N, 144°46.5′E, about 100 km north of Guam, and is a steep-sided basaltic to basaltic-andesite cone with a summit depth of 517 m, a base at 2800 m, and a diameter of 16 km (Figure 1). Explosive eruptive activity at this volcano was first witnessed in 2004 and observed again in 2005 [*Embley et al.*, 2006a]. However, these previous observations were limited by their brief duration and restricted access to the vent. In April 2006, a third dive series found changes had occurred at the vent that allowed better access and unprecedented views of submarine eruptive processes. Video observations at close range over the course of a week documented a diverse and increasingly energetic range of activity that culminated in explosive bursts of glowing red lava propelled by rapidly expanding magmatic gases. In addition, a portable hydrophone deployed near the eruptive vent during some of the dives allowed the visual observations to be correlated to digital acoustic data. Here, we present the video and hydrophone observations and use these data to quantify the eruption rate over time, characterize the style of explosive activity, and present a model for magmatic degassing and magma-seawater interaction witnessed at NW Rota-1. These observations made between 2004 and 2006 are the first direct observations of submarine explosive eruptions ever made.

2. Multiyear Context and Physical Setting

[3] Three separate expeditions made dives at NW Rota-1 volcano with remotely operated vehicles (ROVs) in 2004–2006, after initial mapping and hydrothermal plume surveys in 2003 [*Embley et al.*, 2004; *Resing et al.*, 2008; *Baker et al.*, 2008]. Each ROV survey found the volcano to be

[1]Hatfield Marine Science Center, Oregon State University, Newport, Oregon, USA.
[2]Department of Geological Sciences, University of Oregon, Eugene, Oregon, USA.
[3]Pacific Marine Environmental Laboratory, NOAA, Newport, Oregon, USA.
[4]GNS Science, Lower Hutt, New Zealand.

0148-0227/08/2007JB005215$09.00

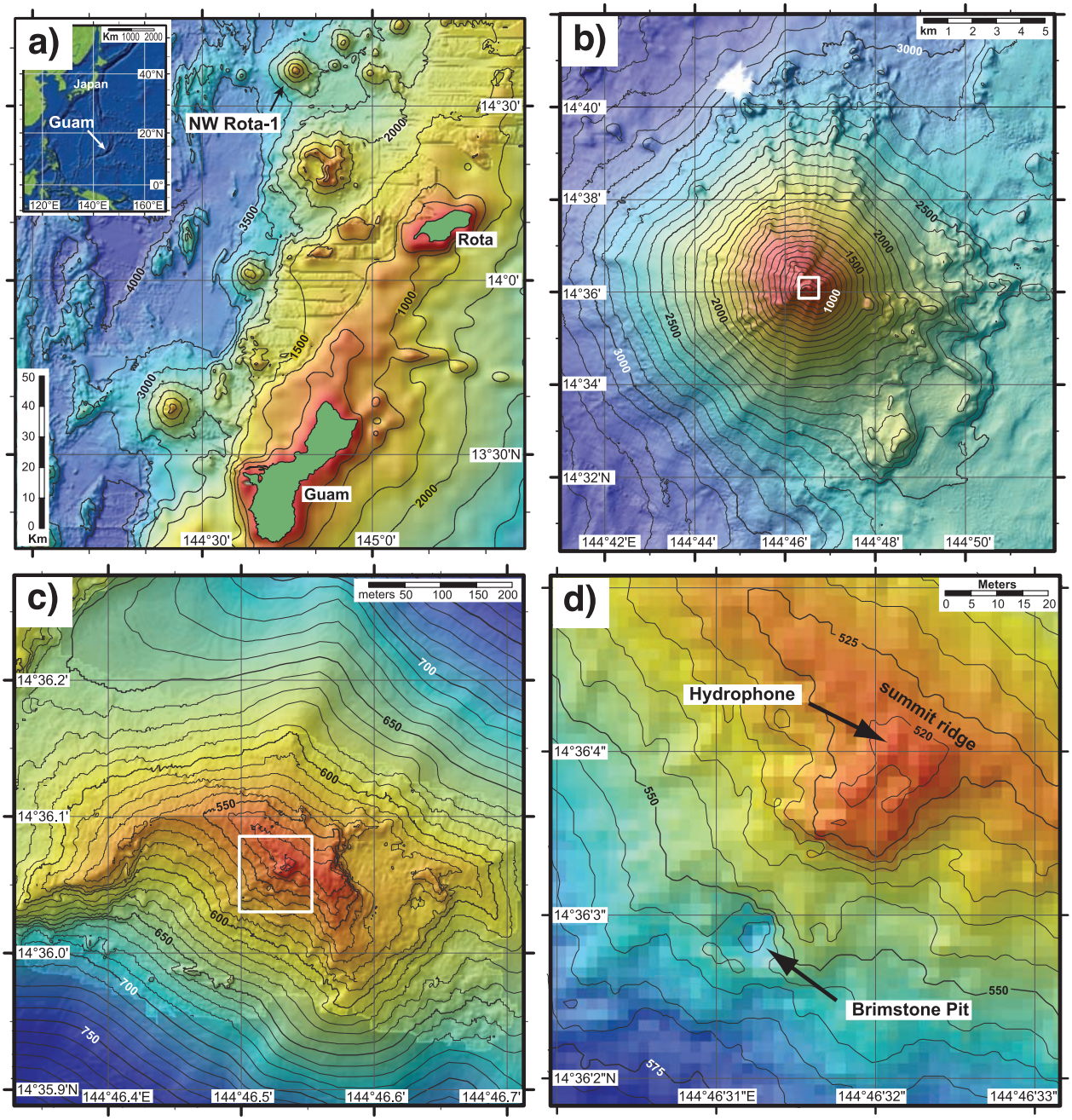

Figure 1. Maps showing the location of NW Rota-1 volcano in the Mariana arc, western Pacific. (a) Regional bathymetry compilation with the islands of Guam and Rota (200-m grid; 500-m contours). (b) EM300 multibeam bathymetry of NW Rota-1 (35-m grid; 100-m contours). (c) Imagenex scanning sonar bathymetry of the summit (2-m grid; 10-m contours). (d) Imagenex bathymetry (2-m grid; 5-m contours) showing location of Brimstone Pit eruptive vent and the volcano summit. Imagenex bathymetry was collected in 2004.

actively erupting, but also documented a different physical setting at the vent, evidence that activity had been ongoing and dynamic between the brief visits. The summit of the volcano was mapped in 2004 with an Imagenex scanning sonar mounted on the ROV *ROPOS* [*Embley et al.*, 2006a], providing high-resolution bathymetry that was processed as described in *Chadwick et al.* [2001]. The active eruptive vent area at NW Rota-1, named "Brimstone Pit," is located about 45 m south of the summit on the steep southern slope of the volcano (Figure 1). The summit consists of an arcuate ridge that is probably the headwall scarp of a landslide, because it is steeper on the concave south side where the slopes are covered with loose volcaniclastic material near the angle of repose. The summit ridge strikes 130° and extends between (and is roughly perpendicular to) inward facing normal faults that strike 030°. These faults are spaced about 800 m apart, have offsets up to 40 m, and cut through the top of the cone. A flat-floored circular depression on the east side of the summit, about 100 m across, may be an old, partially filled crater (Figure 1c). In comparison, Brimstone

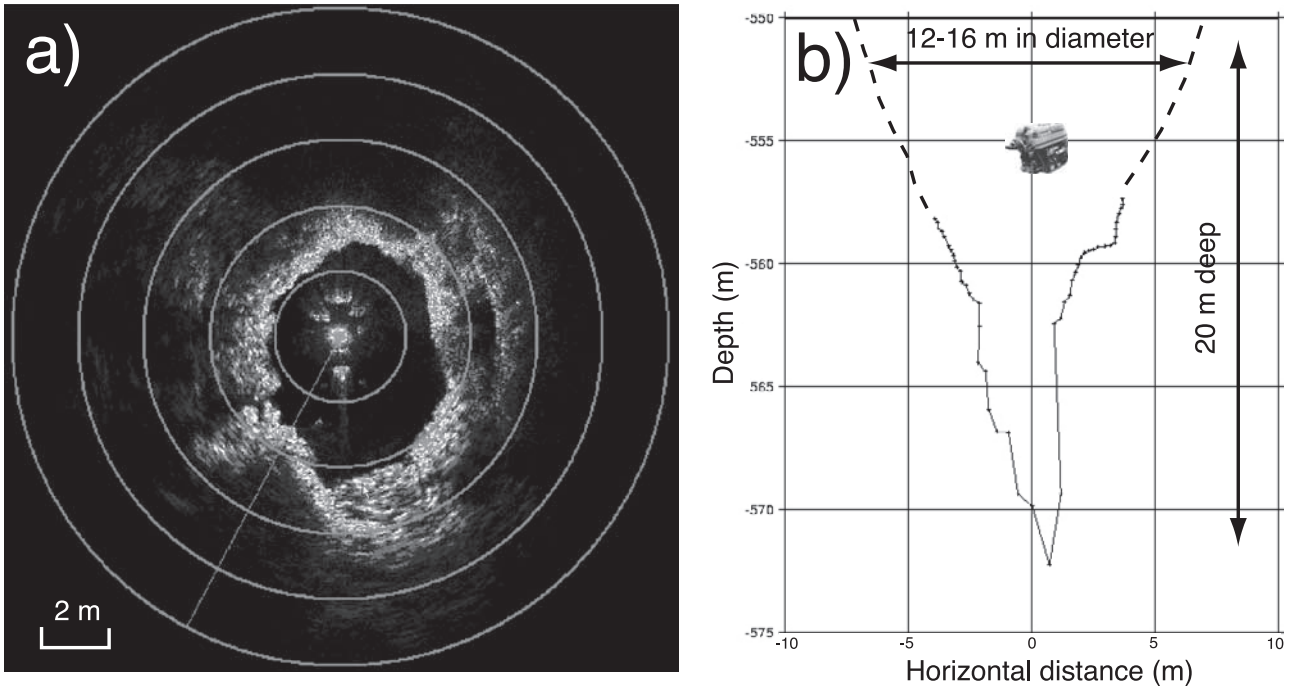

Figure 2. Sonar views of Brimstone Pit in 2004 when a cinder cone existed at the vent. (a) Map view image from sonar on *ROPOS* when it was down inside the crater of the cone (~10 m below the rim) during a prolonged lull in the activity. The ROV is located at the middle of the image and the sonar head scanned 360° in a horizontal plane, showing that the pit was 5–8 m wide at this depth horizon (561 m). (b) Vertical depth profile inside the crater at Brimstone Pit, showing that in 2004 it was conical and ~20 m deep.

Pit is a minor morphological feature, suggesting it is relatively young.

[4] During the first diving expedition in March–April 2004 (on the R/V *Thompson* with ROV *ROPOS*), Brimstone Pit was a crater atop a cinder cone. Scanning sonars on the ROV showed that the pit was 12–16 m wide near the rim, oval in map view, funnel-shaped in profile, and ~20 m deep (Figure 2). The depth of the pit rim varied from 540 to 550 m, with the northern edge merging with a steep slope extending up to the summit. Activity observed in 2004 consisted of occasional pulsing eruptive bursts that ejected ash and lapilli out of the crater along with a thick yellowish plume that contained abundant droplets of molten sulfur [*Embley et al.*, 2006a]. It was not possible to see very far down into the eruptive vent. Water column surveys over the volcano found a hydrothermal plume above the summit similar to the one found the previous year [*Embley et al.*, 2004; *Resing et al.*, 2008; *Baker et al.*, 2008], but also discovered deeper turbidity plumes that extended from 650 m down to at least 2500 m and a distance of 12 km on the volcano flanks [*Walker et al.*, 2008]. These turbid layers contained abundant particles of volcanic glass apparently formed by episodic mass-wasting events of the accumulated eruptive products around Brimstone Pit or by sediment gravity flows during larger eruptions [*Embley et al.*, 2006a; *Walker et al.*, 2008].

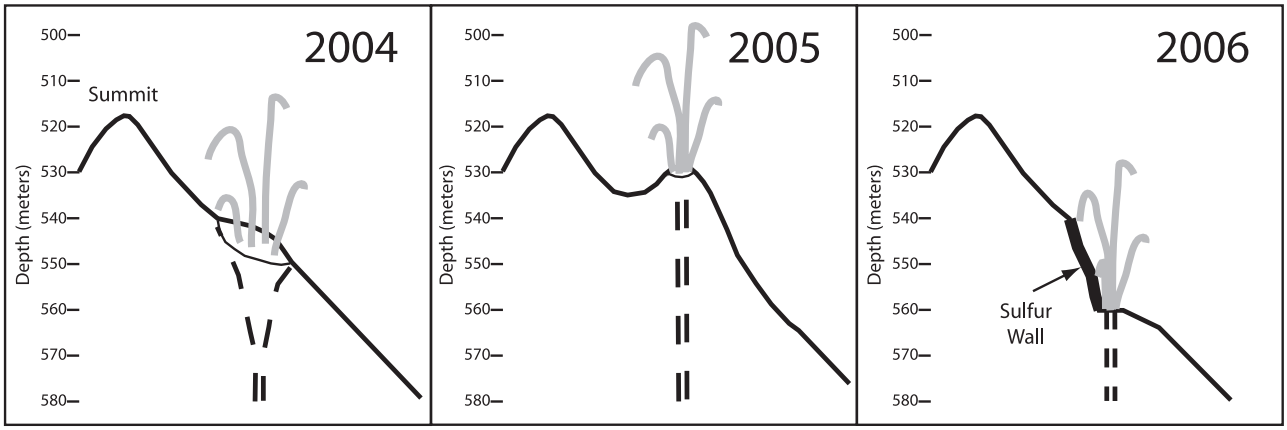

Figure 3. Cartoon cross sections (facing east) showing changes at the Brimstone Pit eruptive vent during 2004–2006. The "sulfur wall" seen in 2006 is interpreted to be a remnant of the inside of the crater seen in 2004.

Table 1. Visual Observations at Brimstone Pit, NW Rota-1, in 2006[a]

		Start		End			
Observation	Jason Dive	Date	Time (UT)	Date	Time (UT)	Duration (h:min)	Comments
1	J2-187	23 April 2006	0918	23 April 2006	1130	2:12	Degassing at exposed vent
2	J2-187	23 April 2006	1636	23 April 2006	1732	0:56	Slow lava extrusion
3	J2-188	24 April 2006	0852	24 April 2006	1052	2:00	Mild explosions
4	J2-189	24 April 2006	2354	25 April 2006	0125	1:31	Mild explosions
5	J2-189	25 April 2006	0528	25 April 2006	0749	2:21	Brief strong explosions
6	J2-191	27 April 2006	0207	27 April 2006	0321	1:14	Sustained strong explosions
7	J2-192	27 April 2006	2029	27 April 2006	2211	1:42	Coincident with hydrophone data
8	J2-192	28 April 2006	0143	28 April 2006	0316	1:33	Coincident with hydrophone data
Total						13:30	

[a]The first dive at NW Rota-1 in 2006 was J2-186, which was near the bottom from 21 April at 2345 UT to 22 April at 0948 UT, but no visual observations were made at Brimstone Pit because of near white-out conditions. Jason dive J2-190 was not at NW Rota-1.

[5] In October 2005, an expedition on the R/V *Natsushima* with the ROV *HyperDolphin* made two dives at NW Rota-1 and found that the active cinder cone at Brimstone Pit had grown upward by 20 m (the depth of the rim was 530 m; Figure 3) and the pit itself was narrower (~5 m) and only a few meters deep [*Embley et al.*, 2006a; *Tamura et al.*, 2006]. This depth change between the 2004 and 2005 dives is accurate because both ROVs measured the same depth (517 m) at the volcano summit. The eruptive activity was similar to that in 2004 but could be observed at much closer range. It consisted of a roiling opaque cloud punctuated by eruptive bursts that threw out rocks and emitted gas bubbles. Ash and lapilli rained down through the water near the eruptive vent and a few sluggish density flows descended the sides of the cone. Deep turbidity plumes were not encountered during the ROV dives, but no water column surveys were collected to confirm their absence.

[6] The April 2006 expedition returned with R/V *Melville* and the ROV *Jason II*. Water column surveys showed deep turbid layers over the flanks of the volcano, as observed in 2004 and extending from 700 m to at least 2900 m depth and 8 km from the summit, again dominated by particles of volcanic glass [*Walker et al.*, 2008]. The turbidity within the plumes diminished substantially within a week. The repeated observation of these deep turbid layers suggests that the eruptive activity at NW Rota-1 in 2004 and 2006 may be characterized by the recurring buildup and collapse of a cinder cone over the vent at Brimstone Pit. Comparison of multibeam bathymetric surveys over the volcano in 2003 and 2006 shows an area of positive depth change up to 40 m, located downslope of Brimstone Pit, consistent with this interpretation [*Walker et al.*, 2008].

[7] In 2006, we appeared to have arrived at NW Rota-1 immediately after one of these collapse events, because initially the turbidity plume was intense and the first ROV dive encountered white-out visibility conditions near the seafloor, but visibility was markedly improved the next day. When Brimstone Pit was located on the second dive, the cinder cone observed in 2004 and 2005 was gone and all that remained was a sulfur-coated wall that was a remnant of the inner slope of the pit (Figure 3). The eruptive vent was at 560 m, 30 m deeper than when it was last observed 6 months earlier, and was now accessible for direct observations. The accuracy of these depth comparisons was again verified relative to the summit. The depth of the vent in 2006 was midway down inside the crater as it appeared in 2004 (Figure 2); most of the cone had been removed, most likely by landslide activity, but the 2004 crater had also been partially filled in.

3. Visual Observations of Eruptive Activity in 2006

[8] Six ROV dives were made over a 7-day period and included eight separate visits to Brimstone Pit. In this section, we describe the visual observations in the vent area and how the eruptive activity evolved over time. The dates and times of the visual observations are shown in Table 1. We also estimate the volumetric eruption rate during and between each visit (Figure 4). The eruption rates were calculated by estimating the volume of the erupted deposits around the vent over time, using ROV video (including a pair of lasers spaced 10 cm apart for scale) and the geometric formula for the volume of a truncated right circular cone. The depth sensor on the ROV was used to determine changes in the height of the cone between visits.

[9] The eruptive activity took place at multiple closely spaced vents within a limited area (~5 × 12 m). Although more than one vent could be active at the same time, one was usually dominant during each visit, and we have named them sequentially as vents A–D below. Each eruptive vent was relatively small (1–5 m in diameter) and successively built

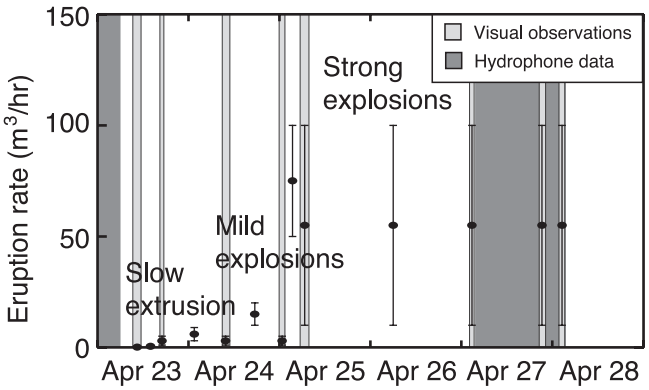

Figure 4. Plot of eruption rate versus time (black dots) during dive series at NW Rota-1 in 2006, showing increase in activity from slow extrusion to strong explosions. Light gray bars denote times when visual observations were made at Brimstone Pit. Dark gray bars denote times when the portable hydrophone was recording. Eruption rates were calculated by estimating the volume of the erupted deposits during and between each visit to the vent.

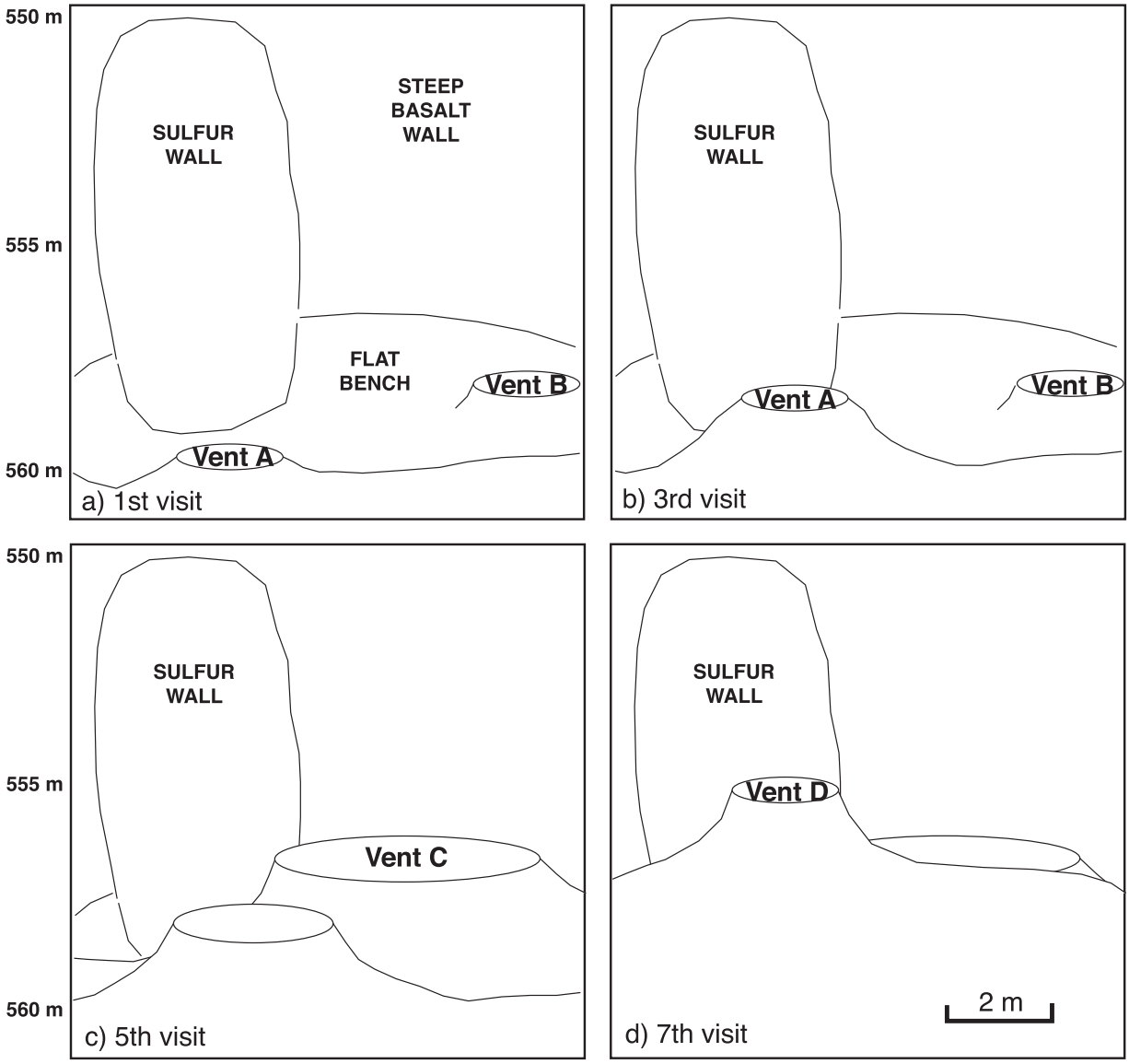

Figure 5. Sketches showing the appearance of the Brimstone Pit area during the 2006 dive series (looking north), emphasizing the changes from visit to visit. The active vents during each visit are labeled vents A–D.

its own tephra cone that overlapped and partially buried previous deposits (Figure 5). As one conduit became plugged, another opened nearby, suggesting that the underlying substrate in the vent area is unconsolidated throat fill.

[10] H_2O, CO_2, and S are the dominant volatiles released from volcanoes [*Wallace and Anderson*, 2000]. For example, lavas sampled at NW Rota-1 contain 1.1–5.8 wt % H_2O, 5–460 ppm CO_2, and up to 1940 ppm S [*Shaw et al.*, 2006]. Magmatic H_2O has the greatest potential for volume expansion as it flashes to steam when pressure is released at the eruptive vent. Underwater, CO_2-dominated gases are emitted as bubbles that can be easily distinguished from sulfur-dominated particle plumes because they are clear and more buoyant, and they physically separate from the sulfurous clouds due to their faster ascent rate [*Butterfield et al.*, 2006]. When sulfur-dominated gases such as SO_2 and H_2S exsolve from magma and mix with seawater, they react to form tiny droplets of molten sulfur in a cloudy particle plume [*de Ronde et al.*, 2005; *Embley et al.*, 2006a; *Butterfield et al.*, 2006]. In the following, we refer to CO_2 bubbles and S particle plumes, referring to their dominant constituents while acknowledging that other gases and particles may also be present. More information on fluid, particle, and gas compositions at NW Rota-1 is provided by *Butterfield et al.* [2006], *Resing et al.* [2008], and D. A. Butterfield et al. (Magma degassing, acid alteration, and metal volatility at the actively erupting NW Rota-1 submarine volcano, Mariana arc, manuscript in preparation, 2008).

3.1. Dive J2-186

[11] During the first ROV dive, a cloud much larger than any encountered at the site before or since enveloped the entire summit and reduced visibility to near zero. The cloud was milky white and similar to those previously encountered that contained abundant tiny sulfur particles (Figure 6a and Movie 1[1]). Apparently a large eruptive

[1]Animation X is available in the HTML.

event had just occurred, perhaps related to removal of the preexisting cinder cone. The cloud was at least 400 m across (and probably more) with a distinct upper limit at a depth of ~470 m (50 m above the summit and 90 m above the vent). The ROV approached Brimstone Pit from each quadrant, but the visibility was so poor (<2 m) that the eruptive vent could not be located. Ash and lapilli were seen falling through the water, evidence that eruptive activity was occurring during the dive. In addition, streams of CO_2 bubbles rose through the white sulfur-dominated particle plume directly over the vent. However, when the portable hydrophone was deployed several hours into the dive (see section 4), it recorded few acoustic events, suggesting that the eruptive activity that created the plume had waned greatly by the start of the dive.

3.2. Dive J2-187

[12] Seventeen hours later during the second dive, visibility had greatly improved and we visited Brimstone Pit twice after recovering the portable hydrophone from the summit. The ROV approached Brimstone Pit from the south, moving up a 35° slope covered by recent ejecta from the vent, a mixture of ash, lapilli, and bombs mostly 10–50 cm in diameter (but up to 1 m), dusted with tiny sulfur globules (a few millimeters across) that originate as droplets of molten sulfur [*Embley et al.*, 2006a; *Butterfield et al.*, 2006]. The fine, light-colored sulfur beads are much less dense than the other volcanic ejecta and concentrate on the surface like a layer of powdery snow. The slope below Brimstone Pit is marked by distinct slide chutes up to 5 m wide, defined by abrupt changes in color and average clast size. Most of the volcanic bombs on the slope were dark and fresh, but a few were light gray colored, apparently due to alteration in the vent or within the volcanic conduit. Many bombs had vesicles that were completely filled with sulfur, while other blocks were entirely composed of sulfur, sometimes appearing as long, sinewy strands that formed when the sulfur was molten (N. D. Deardorff et al., Observations of eruptive plume and pyroclastic deposits from submarine explosive eruptions at NW Rota-1, Marianas Arc, manuscript in preparation, 2008).

[13] During the first visit to Brimstone Pit, the active vent ("Vent A") was only discharging a weak plume, which allowed us to examine the new surroundings (Figure 5a). The vent area was located on a bench ~5 m wide and ~12 m long cut into the steep slope. Just behind and upslope of Vent A was an arcuate, near-vertical wall composed of welded volcanic ejecta coated with a veneer of bright yellow sulfur (Figure 6b and Movie 2). Above this wall, the slope continued upward over craggy outcrops toward the summit. The sulfur wall was 10 m high, 5 m wide, and 1 m thick (when viewed from the side) and was apparently a remnant of the inner crater of the cinder cone that had previously existed. Now, the cone had been removed and the vent was simply a shallow basin of rubble, ~2 m across and ~1 m deep, with a central area ~1 m across (Figure 6c and Movie 2).

[14] Although Vent A appeared to be the primary eruptive vent, we later discovered that another vent (Vent B) located ~6 m east on the bench was also occasionally active. At times when we were observing Vent A, an eruptive cloud from nearby (but unseen) Vent B would drift in, raining down ash and temporarily obscuring visibility. Vent B became dominant during later dives but eventually activity shifted back closer to the sulfur wall with Vents C and D (Figure 5).

[15] Initially, Vent A was not erupting and little degassing was occurring. After 50 min of observation at Brimstone Pit with no visible CO_2 gas streaming, bubbles gradually appeared. The rate of degassing increased over the next 1.5 h until bubbles were rising in continuous streams from the vent area (Figure 6d and Movie 2). During this time the sulfur-dominated particle plume also became thicker. The dramatic increase in degassing was due to magma slowly rising in the conduit, as we discovered when we next returned.

[16] During the second visit, 5 h later, we discovered lava slowly extruding in pulses from the vent, each pulse accompanied by strong degassing (Figure 6e and Movie 3). A thick plume, ~1 m in diameter at the base, rose from dark angular blocks of new lava that had extruded since the first visit. The total volume of extruded material was estimated at ~1–5 m^3, yielding an average eruption rate of $\leq$1 m^3/h. A cyclic pattern of degassing and eruption became apparent with vigorous CO_2 discharge preceding lava extrusion by 5–15 min, then a thick yellowish (sulfur-dominated) cloud would accompany extrusion (coming directly off the new lava) for 15–30 min (Figure 6f and Movies 4 and 5), followed by a lull of 5–15 min with greatly diminished degassing (Figure 6g). At the onset of one of these cycles, the rate of CO_2 release increased very rapidly from just a few bubbles to sheets and clouds of bubbles within a few minutes. By the time lava extrusion started, CO_2 output was waning, and sulfur degassing became dominant, though for 5–15 min both occurred together. Soon, however, CO_2 bubbles diminished, followed 15–30 min later by the dissipation of the sulfur cloud. Thus, the most intense CO_2 output was in the minutes just *before* lava extrusion, whereas the most intense (and brightest yellow) sulfur emissions occurred *during* the first minutes of extrusion. This timing is consistent with the lower solubility of CO_2 compared with H_2O or S, causing it to exsolve from the magma at greater depths than either H_2O or

Figure 6. ROV video frames showing activity at Brimstone Pit during visits 1–4 in 2006. (a) A large eruptive cloud covered the entire summit on the first dive; white dots are gas bubbles (see Movie 1). (b) On the first visit to Brimstone, most of the former cone was gone except for a sulfur coated remnant of the inner crater wall (middle left) behind the eruptive vent (lower right). (c) At first, Vent A was only weakly smoking. (d) Later it began to vigorously emit CO_2 bubbles (see Movie 2). (e) During the second visit, lava was passively extruding and degassing in the vent (see Movie 3). (f) Yellow-tinged sulfur-rich particle plumes emanated directly from the new lava. (g) Within ~30 min after extrusion, most degassing had stopped (see Movies 4 and 5). (h) A day later, during the fourth visit to the vent, explosive activity had started at Vent A (see Movie 6). Numbers along top of images show dive number, date, time, heading, and depth (m). Red lasers are 10 cm apart.

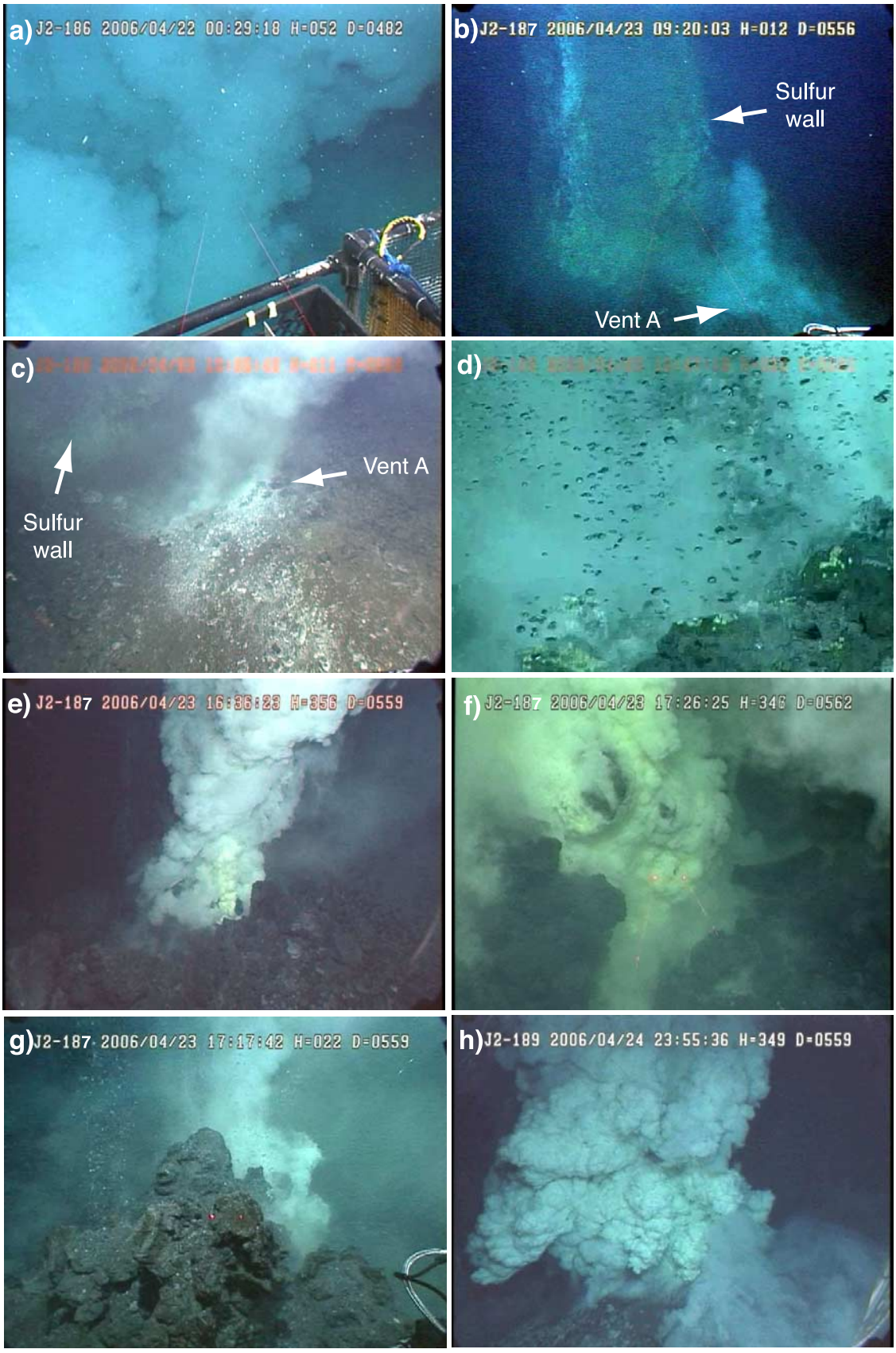
a) J2-186 2006/04/22 00:29:18 H=052 D=0482
b) J2-187 2006/04/23 09:20:03 H=012 D=0556
Sulfur wall
Vent A
c)
Vent A
Sulfur wall
d)
e) J2-187 2006/04/23 16:36:23 H=356 D=0559
f) J2-187 2006/04/23 17:26:25 H=346 D=0562
g) J2-187 2006/04/23 17:17:42 H=022 D=0559
h) J2-189 2006/04/24 23:55:36 H=349 D=0559

Figure 6

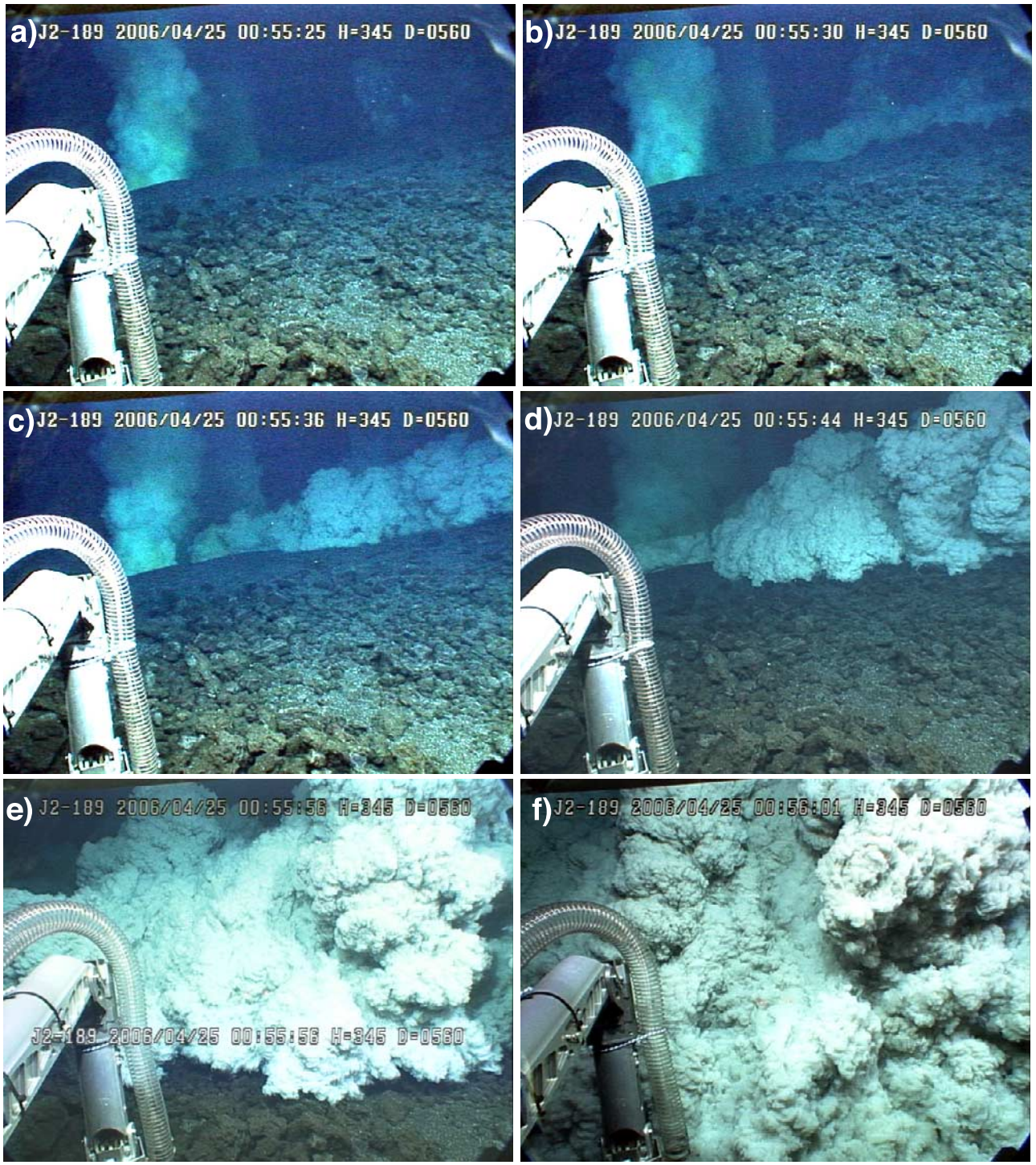

Figure 7. ROV video frames during the fourth visit to Brimstone Pit in 2006 showing a sudden explosive burst from Vent B (upper right) that generated a short-lived, dilute density flow, contrasting with the more continuous activity at Vent A (upper left). The ROV was looking upslope from a location about 10 m away from the two vents (see Movie 7). Elapsed times are (a) 0 s, (b) 5 s, (c) 11 s, (d) 19 s, (e) 31 s, and (f) 36 s.

S [*Wallace and Anderson*, 2000]. The rate of degassing peaked and declined quickly. An area that was intensely degassing and generating a thick plume one minute could have no signs of degassing 30 min later. During this second visit to the vent, we observed about 1 m^3 of new lava extruded in about 15–30 min with no explosive activity (a rate of ~2–4 m^3/h).

3.3. Dive J2-188

[17] Fifteen hours later (Table 1), during the third visit, the vent had changed again (Figure 5). Light gray clastic

deposits (mostly ~1 cm in size, but up to 10 cm) now covered the blocky lava seen on the previous dive, evidence that explosive activity had started. The rim of the vent was at 558 m, and the vent was vigorously degassing CO_2 bubbles and white/yellow sulfur plumes. The CO_2 bubbles were emitted through the permeable clastic deposits further from the vent than the sulfurous plume. The near-vent deposits were 1–2 m thick and 3–5 m across, suggesting an eruption rate since the last visit of ~5 m^3/h.

[18] During this visit, cycles of CO_2 and sulfurous plume degassing waxed and waned every 5–15 min. The visibility was variable so it was sometimes difficult to see what was happening in Vent A, partly because plumes from the neighboring Vent B appeared every 30–60 min, accompanied by ashfalls. Toward the end of this visit, minor explosive bursts were observed within Vent A at the base of the plume. Each burst lasted a few seconds and generated a dark roiling ash-filled plume (~10 cm across) that was quickly incorporated into the larger light colored sulfurous plume generated from the ongoing degassing. These explosive bursts were separated by intervals of 10 s up to several minutes. During this dive, activity was characterized by intermittent low-level explosions with an eruption rate estimated at ~1 m^3/h.

3.4. Dive J2-189

[19] The fourth visit to Brimstone pit was ~13 h later. A circular tephra cone made of relatively fine-grained clasts (~1 cm) had built up around Vent A. The rim of the growing cone was ~1 m higher (now at a depth of 557 m) and wider (2–3 m across at the rim) than on the previous visit, suggesting the eruption rate had increased to 10–20 m^3/h between visits. A thick billowy white plume rose from the vent and mild ash explosions could be seen in the core of the plume (Figure 6h and Movie 6). The ejecta from the explosions were up to fist-sized and mostly fell back into the vent and onto the rim of the cone. Carbon dioxide bubbles rose out of the billowing clouds of individual explosive bursts as solid ejecta fell out below. After ~20 min of this activity, a lull ensued that lasted for ~30 min, and we could see that the vent (the area from which plumes were discharged) in the bottom of the crater was ~0.6 m in diameter and about 1 m below the rim of the tephra cone.

[20] During this lull, the ROV moved downslope ~10 m to test a new sampler. We were looking upslope, when Vent A began to erupt again with mild explosions at the base of a vertically rising plume, as before. However, about 35 s later, Vent B erupted suddenly with much more vigor and created a cloud that quickly moved outward in all directions as a dilute density flow (Figure 7 and Movie 7). The high bulk density of the ejected material apparently caused the plume to collapse quickly, generating a ground-hugging gravity flow composed of fine ash and sulfur particles that traversed the 10 m to the ROV in 35 s (~0.3 m/s). The density flow was ~2 m thick and quickly lost momentum by the time it reached the ROV. This confirmed the existence of multiple, closely spaced eruptive vents for the first time, and showed that they could erupt simultaneously and yet exhibit different eruption rates and styles. This burst from Vent B was apparently due to trapped gases suddenly breaking through a plug of solidified lava in the vent (an unsustained phase lasting only ~5 s). The average eruption rate overall during this fourth visit was estimated at 1–5 m^3/h.

[21] The ROV then moved away from Brimstone Pit for 4 h, and when it returned for a fifth visit the appearance of the vent had again changed dramatically (Figure 5). The active vent (Vent C) was now located between Vents A and B, and had grown higher by 1 m and wider (~5 m). This showed that the eruption rate had increased to between 50 and 100 m^3/h since the previous visit, based on the volume of the new deposits. Small flows of molten sulfur extended from the sulfur wall down into Vent A, apparently melted and remobilized by eruptive activity at Vent C. The style of activity had also changed. Vent A was mostly inactive and only weakly discharging a plume. Instead, major degassing was occurring from Vent C and extended several meters down the flanks of its tephra cone. Curtains of CO_2 bubbles extended outward from the vent beyond the sulfur-dominated plumes. The boundaries of these "degassing fronts" on the sides of the cone had a lobate pattern and were so distinct that, at the time, we misinterpreted them to be flow fronts of thin sluggish lava flows descending the sides of the cones (Figure 8a and Movie 8). However, analysis of the ROV video shows that the gases were rising through clastic material, and that the "degassing fronts" actually advanced and retreated slightly up and downslope on the cone over 10s of minutes. We now interpret that the wider area of degassing during this time (up to 10 m wide) resulted from gas release taking place beneath the seafloor and rising through the conduit walls and the permeable cone (in contrast to most other times when degassing originated in the vent). Small (rootless?) explosive bursts of roiling ash emanated from the flanks of the cones in some of these degassing areas. At the same time, nearly continuous low-level explosions that generated ash and lapilli were occurring inside the cone of Vent C. These explosions continued for ~1 h and were accompanied by streams of CO_2 bubbles and roiling bright yellow clouds (Figure 8b and Movie 9).

[22] Near the end of this fifth visit, explosive activity intensified further and short strong bursts threw fragmental

Figure 8. ROV video frames and digital still camera images showing activity at Brimstone Pit during visits 5–8 in 2006 (dive numbers and times indicated if missing from image). (a) Lobate pattern of prolonged degassing through the flanks of the tephra cone at Vent C during the fifth visit (see Movie 8). (b) Yellow sulfur-rich explosive degassing from Vent C (J2-189, 0703:23 UT) (see Movie 9). (c) Stronger but brief explosive burst at the end of the fifth visit (see Movie 10). (d) During the sixth visit, multiple vents were located adjacent to the sulfur wall (see Movie 11). (e) Bubbles of CO_2 are visible in front of a sulfurous eruptive plume in the background (J2-191, 0259:38 UT). (f) By the seventh visit, the eruptive vent (Vent D) had moved away from the sulfur wall again (see Movie 12). (g) The explosive bursts were sustained for several minutes at a time (J2-192, 2115:34 UT). (h) Erupted material could slide directly from the vent (upper right) down the steep southern slope, at left (J2-192, 2139:36 UT).

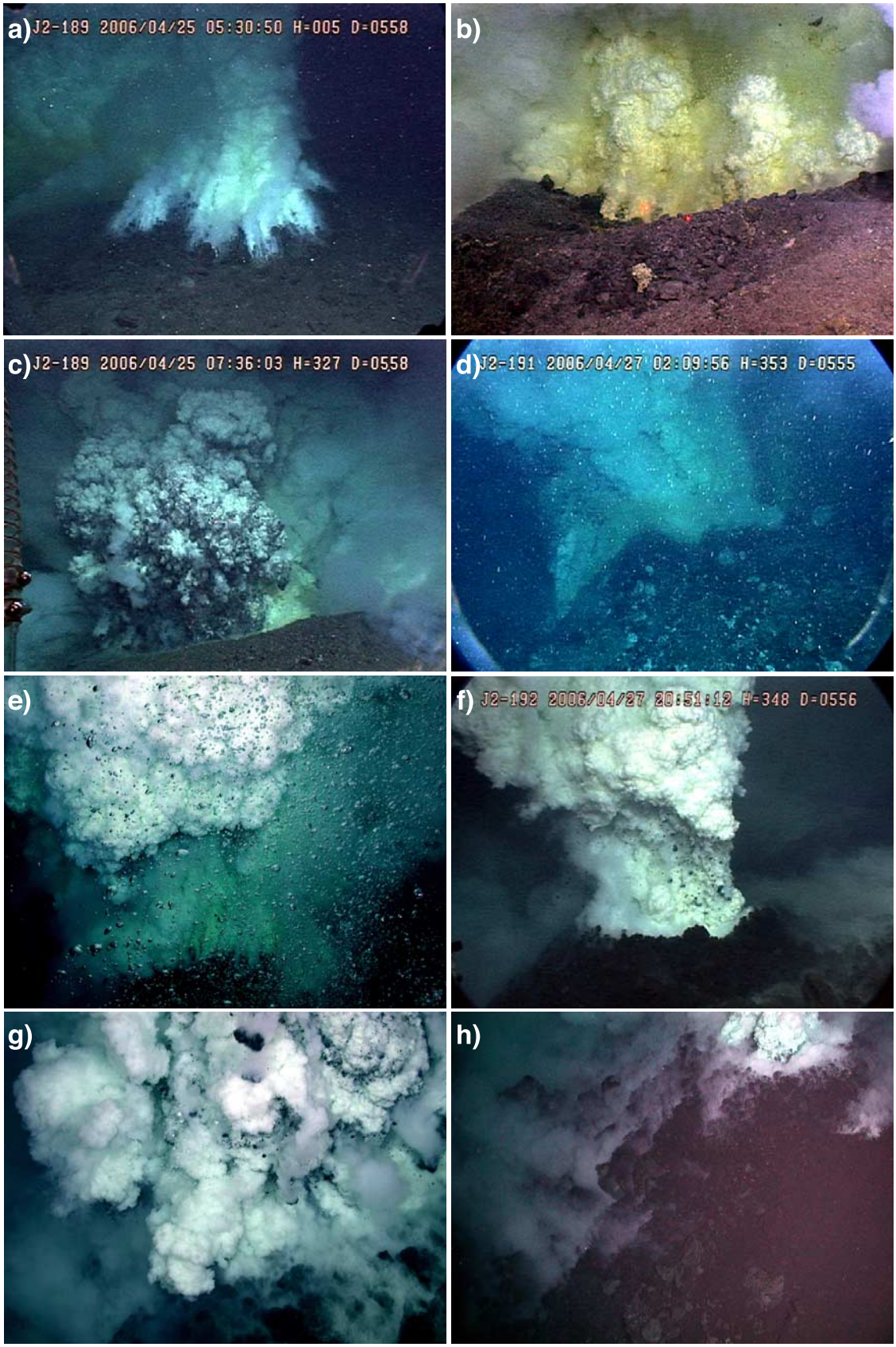
a)
J2-189 2006/04/25 05:30:50 H=005 D=0558
b)
c)
J2-189 2006/04/25 07:36:03 H=327 D=0558
d)
J2-191 2006/04/27 02:09:56 H=353 D=0555
e)
f)
J2-192 2006/04/27 20:51:12 H=348 D=0556
g)
h)

Figure 8

lava at least 2 m above the vent (Figure 8c and Movie 10). Each burst lasted only 5–20 s and comprised multiple pulses that fed a continuous sulfurous plume. Ash and bombs were driven upward by the explosions for a second or two, before rapidly decelerating and falling back down out of the plume and into the vent or onto the rim of the cone (N. D. Deardorff et al., manuscript in preparation, 2008). The individual bursts were separated by pauses lasting 20–60 s. These explosive bursts continued for 10 min before the dive ended. We estimate an eruption rate of 10–100 m^3/h during this fifth set of observations, a significant increase that would continue during the next two dives (Figure 4).

3.5. Dive J2-191

[23] The sixth visit to Brimstone Pit was made after an absence of 42 h (dive J2-190 was made at neighboring Esmeralda Bank volcano). During the approach to the vent, the ROV encountered a thick plume containing ash and sulfur beads that dissipated after 10s of minutes. Closer to the vent, the recently erupted volcanic ejecta was much coarser (10–50 cm) than had been observed previously. The active eruptive vent had changed slightly and the western end of Vent C was now studded with multiple small craters (each ~1 m in diameter), located up against the eastern half of the sulfur wall (Figures 8d and 8e). This line of vents (at 553 m) was 4 m shallower than the remnants of Vent A (Figure 5). Volume calculations suggest the eruption rate had continued at its elevated level of 10–100 m^3/h since the last visit. This high level of activity deposited more material than the bench could hold, resulting in pyroclastic debris episodically moving down the steep southern slope. This meant that estimating the eruption rate between visits from the volume of new deposits was no longer possible; after this time eruption rate estimates are based solely on the video observations (Figure 4).

[24] During much of this sixth visit, low-level explosive activity from multiple craters was intermittently punctuated by larger bursts that expelled fist-sized bombs and sometimes generated laterally expanding plumes that temporarily enveloped the vehicle (Movie 11). Consequently, visibility was often marginal, although individual vents could be seen to have grown in height during the visit. We estimate the eruption rate continued at 10–100 m^3/h. Immediately after this visit to Brimstone Pit, the portable hydrophone was deployed at the summit for the second time.

3.6. Dive J2-192

[25] The two visits to Brimstone Pit during dive J2-192 were the first with simultaneous portable hydrophone recording and visual observations at the vent. The seventh visit to Brimstone began 17 h after the previous visit (Table 1). These observations are the best of the dive series because the visibility was particularly good and the activity was at its peak. The rim of the active cone (Vent D) was 2 m lower (555 m) than on the previous dive because of substantial removal of the near-vent ejecta by slides, but was still 5 m higher than on the first visit. The vent had also moved further away from the sulfur wall and had a single crater 1–2 m wide in a cone made of loose fist-sized bombs (Figures 8f and 8g). The south side of the cone merged with the slope below and ejecta could now move from the vent directly down the steep south slope (Figure 8h).

[26] The eruptive activity was characterized by sustained explosive bursts each lasting several minutes and separated by short intervals of 10–100 s. This pattern of bursts and pauses continued throughout the entire visit, with 18 bursts in 1 h and 42 min. During the pauses, low-level passive degassing formed a gently billowing white plume above the vent (Figure 9a). Each burst began abruptly with a sudden increase in the rate and intensity of degassing (Figure 9b and Movie 12), often accompanied by a surge in CO_2 bubbles and sulfur, the latter evidenced by a distinct yellowing of the particle plume. At the same time, pyroclasts began to be ejected from the vent, mainly seen falling from the periphery of the roiling opaque cloud. About 30 s after the start of most bursts, a large plug of lava was pushed up in the vent (Figure 9c) and was blown apart by vigorous explosions (Figure 9d and Movie 12). The plugs appeared to be solidified caps at the top of the magma column that partially trapped pressurized magmatic gases below (Movie 13). Some plugs cracked open and unfurled almost like the petals of a flower. Parts of the disintegrated plug were thrown upward, often as flat disc-shaped bombs up to 50 cm across, while others tumbled down the sides of the cone as large blocks and slabs (N. D. Deardorff et al., manuscript in preparation, 2008). The intensity of the explosive activity within a burst became distinctly higher after the disruption of the lava plug and this higher level was usually sustained for the remainder of the burst. At the end of a burst, explosive activity abruptly shut off and the vent returned to a state of passive degassing (Movie 12).

[27] Within a burst, each explosive pulse formed a rapidly expanding cauliform protrusion in the billowing eruptive plume, out of which CO_2 bubbles rose and fragmental lava fell out. It was rare to see actual clasts being ejected upward, as this typically occurred within the obscured interior of the plume. The largest bombs decelerated rapidly due to the drag of moving through seawater and fell back in, or near, the vent. Smaller ash and lapilli could be carried both vertically and laterally for tens to hundreds of meters, judging from our encounters with eruptive plumes and the distribution of recent ejecta on the seafloor around the summit of the volcano. For example, the hydrophone was covered by ~0.5 cm of ash and lapilli after being deployed at the summit for 1 day. We estimate that each burst erupted about 1–5 m^3 of lava, which is within the previously estimated range of 10–100 m^3/h (Figure 4).

[28] In many explosive bursts, the outer perimeter of gas emission through the permeable tephra cone would "pulse," heaving outward and inward by ~10 cm at a rate of about once a second, most likely reflecting pressure oscillations within the shallow conduit. At other times, rocks in the vent and on the sides of the cone could be seen shaking, and sometimes the eruptive plume itself would also "pulse," expanding and contracting 5–10 times a second (Movie 14). During the most energetic explosive bursts, flashes of glowing red lava could be seen in the core of the plume up to many times a second (Figures 9e and 9f and Movie 15). In these instances, molten lava was being erupted at a rate faster than seawater could cool the surface below the temperature of incandescence (~700°C).

[29] These observations can be used to estimate the instantaneous eruption rate when red glow was visible. From the video, we estimate that the volume of glowing lava at any

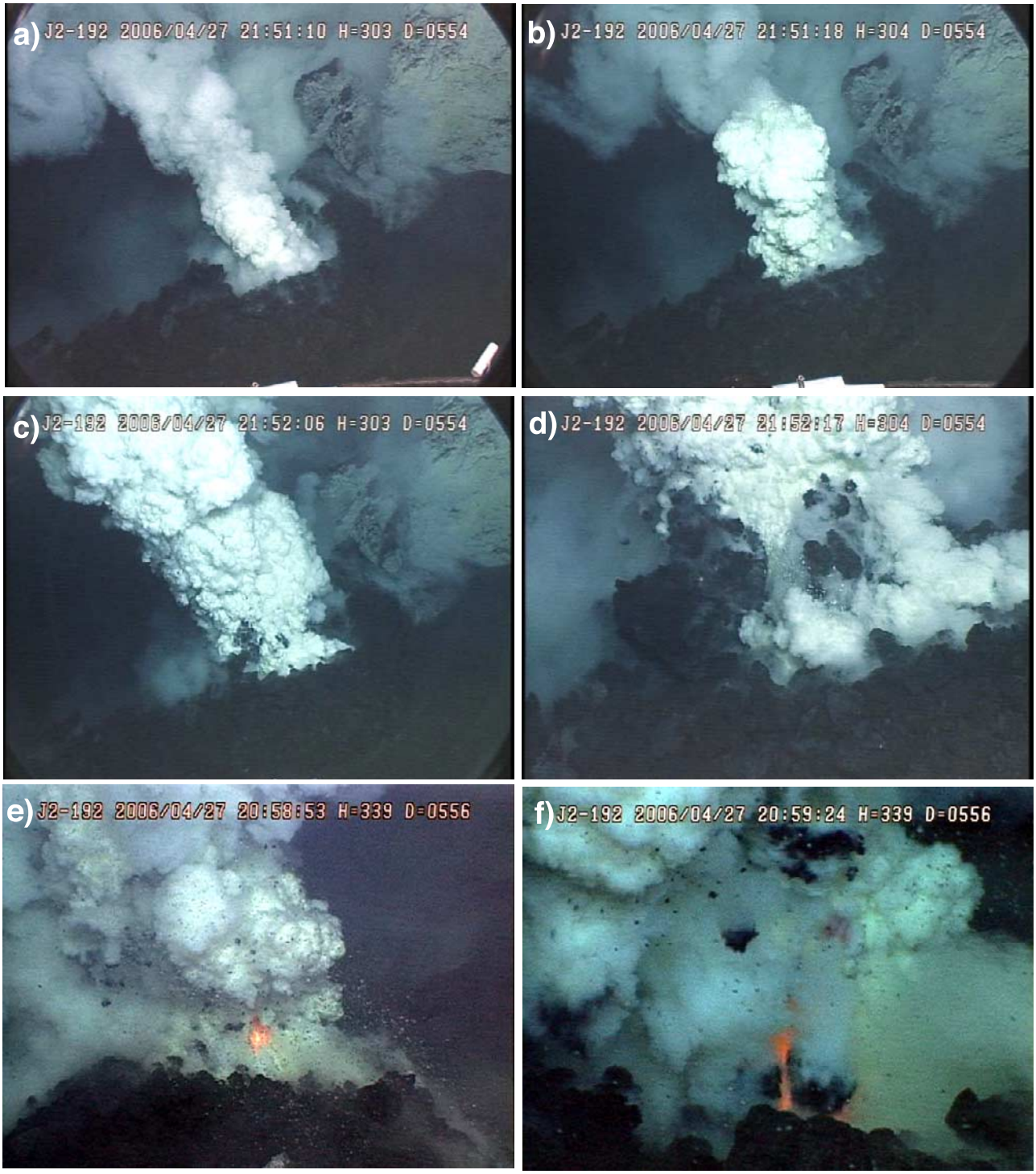

Figure 9. Typical sequence of an explosive burst during the seventh visit to the vent. (a) Noneruptive pause between bursts. (b) Abrupt start of an eruptive burst with a surge of degassing (see Movie 12). (c) After ~30 s, a solidified plug is forced upward in the vent. (d) The plug is blown apart by violently expanding gases (see Movie 13). (e and f) During the most intense explosive bursts flashes of glowing lava were observed in the core of the plume (see Movies 14 and 15).

one instant was a cylinder about 10 cm in diameter and 30 cm in height. By studying the video frame-by-frame, we find that the duration of the glow is typically 1–3 frames (0.03–0.1 s), consistent with previous numerical modeling that shows that cold seawater should cool a molten lava surface from 1100°C to 700°C within about 0.1 s [*Griffiths and Fink*, 1992; *Gregg and Fornari*, 1998]. Therefore, if we assume that the full height of the 30-cm-high cylinder of glowing lava must be extruded within 0.03 s that translates to an eruption velocity of 10 m/s, or an eruption rate of 0.08 m^3/s (or ~300 m^3/h). This instantaneous eruption rate is 3–30 times higher than the average rate we calculated by estimating the volume of

Table 2. Portable Hydrophone Recordings at Brimstone Pit, NW Rota-1, in 2006[a]

Deployment	Dive on Which Deployed	Recording Start		Dive on Which Recovered	Recording End		Recording Duration (h:min)
		Date	Time (UT)		Date	Time (UT)	
1	J2-186	22 April 2006	0202	J2-187	23 April 2006	0605	28:03
2	J2-191	27 April 2006	0341	J2-192	28 April 2006	0339	23:58
Total							51:01

[a]Note the times above are the start and end of useful acoustic data. The hydrophone was also recording before and after these times while it was in the Jason II basket, but these intervals are not included, because the data are not useful due to severe interference from vehicle noise.

ejecta erupted. However, these instantaneous rates were not sustained and represent brief instances of maximum ejection velocities. Nevertheless, this gives an upper limit for the eruption rate at Brimstone Pit during our observations in 2006. By way of comparison, this mass eruption rate is similar to typical rates documented on land during Strombolian eruptions [*Vergniolle and Mangan*, 2000].

[30] The ROV then conducted work away from the vent for 3.5 h before returning for the eighth and final visit (Table 1). During these last observations, the eruptive activity was similar to that observed earlier in the dive, although the visibility was considerably worse and the vent was often obscured from view. We estimate that the eruption rate remained about the same as during the previous visit (Figure 4). At the end of the dive, the portable hydrophone was recovered at the summit from its second deployment.

3.7. Summary of Visual Observations

[31] The eruptive activity we observed evolved from extrusive to explosive. The duration of the explosive bursts were relatively long compared to the intervals between them, and the eruption rate and the intensity of the bursts generally increased over time. The eruptive bursts were mainly driven by expanding magmatic gases. The size of the ejecta thrown out of the vent coarsened with time. All the pyroclastic ejecta had cooled by the time it landed; we saw no evidence of agglutination or welding. Indeed, much of the erupted material intermittently slid down the south slope of the volcano.

4. Hydroacoustic Observations of Eruptive Activity in 2006

[32] We used a small portable hydrophone to record the sounds of the eruption during two deployments at the summit at a depth of 517 m, ~60 m (slant range) from Brimstone Pit (Figure 1). We used a "B-Probe" hydrophone from Greeneridge Sciences that was originally designed for marine mammal studies. It is compact, self-contained (~20 cm long) and has a 16-bit data logger with a dynamic range of 96 dB (however, the system's internal noise limits this to a somewhat lower level). The hydrophone's sensitivity was −170 dB relative to 1 V/μPa. The B-Probe has 1 pole high-pass filters at 5 and 8 Hz to eliminate unwanted ocean surface wave noise, and a sample-rate-dependent low-pass filter to avoid antialiasing (set at 1727 Hz in our deployments). The B-Probe can be programmed to record at a user-specified sampling rate, which determines how long it takes to fill the available memory. We recorded at 4681 Hz for ~30 h during the two deployments at the beginning and end of the dive series (Table 2). The B-Probe's realtime clock has an accuracy of ~1 s/d and was manually set before each deployment. The hydrophone was deployed in a bracket on a small cement pad weighing ~10 pounds in our deployments. We found that no useful data were recorded while the hydrophone was carried by the ROV due to vehicle noise and vibration (even when the ROV was right next to the vent). Once the hydrophone was deployed on the seafloor, however, there was little or no acoustic interference from the ROV or the ship.

[33] The data from the two deployments are very different from one another in that the first recording is very quiet, mostly low-amplitude ambient noise, while the second recorded nearly continuous explosion signals (Figure 10). This is mainly because the first deployment was during the lull that we interpret to have followed the large eruptive/landslide event that created the cloud over the summit and the deep turbidity plume around the flanks of the volcano. In contrast, the second hydrophone deployment was made during the peak of eruptive activity during the last two dives. The first record has some signals that are eruptive in character (57 identified events in ~28 h), although most of these are in the first quarter of the record and are very low in amplitude compared to those in the second recording. There were no observations at Brimstone Pit during the first hydrophone record, but the vent was only weakly discharging when it was first seen ~3 h after the B-Probe was recovered.

[34] The simultaneous audio and video observations of the explosive activity during the seventh and eighth visits to the vent make it possible to directly relate physical processes with acoustic events. Since the hydrophone data extend over a much longer time period than the brief ROV visits, they also provide information on activity at the vent when the ROV was not present. The acoustic data make it possible to quantify the character of the eruptive activity, including the duration and frequency of eruptive bursts and pauses, the relative intensity of each burst, and how these changed with time. Consequently, the remainder of this section will focus on the second hydrophone record.

[35] The second hydrophone record is characterized by a series of acoustic pulses separated by shorter, quieter intervals. Comparison with the ROV video shows that the acoustic events correspond exactly in time with the explosive bursts observed at the vent, and the quiet intervals with the noneruptive intervals. The hydrophone recorded 293 explosive bursts over a ~24-h period, or an average of one every 5 min. The bursts range in duration from 21 to 656 s, with a mean of 245 ± 121 s and a mode of 160 s (Figure 11a). The pauses range in duration from 2 to 270 s, with a mean of 47 ± 35 s and a mode of 35 s (Figure 11b). The character of the bursts also changed over time. For example, during the first 7 h (until 1100 UT on

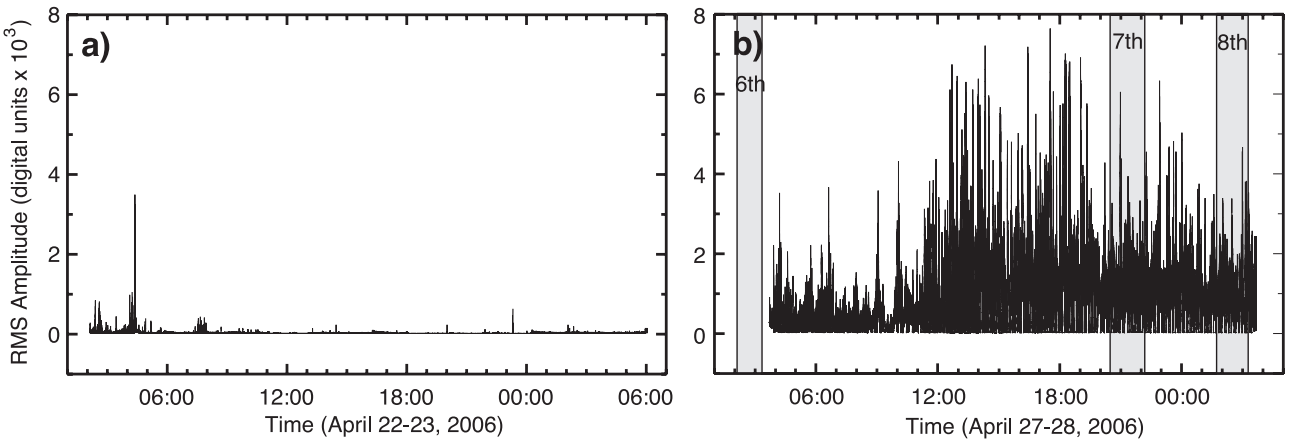

Figure 10. RMS acoustic amplitude measured by the portable hydrophone during the (a) first and (b) second deployments, showing the large increase in activity between the two. RMS amplitude is shown in digital units, averaged every second. Grey bars in Figure 10b show the times of the sixth, seventh, and eighth ROV visits to Brimstone Pit.

27 April), the bursts were not easily distinguished from the pauses because the bursts were longer and lower in amplitude and the pauses were not completely quiet (Figure 12a). Moreover, the transition between bursts and pauses was somewhat gradual and continuous. In contrast, during the last 17 h of the hydrophone recording, the bursts were better defined, because their amplitude was higher, the pauses between them were shorter and quieter, and the transitions were more abrupt (Figure 12b). This can also be seen in a plot of sound pressure level versus time (Figure 13a); after 1100 UT on 27 April the sound levels of the bursts and pauses are more distinct, because the sound level increased during the bursts and decreased during the pauses. Within each of these contrasting intervals, the duration of the bursts increased with time, and there was a sharp decrease in duration at around 1100 UT when the change in character occurred (Figure 13b).

[36] The frequency content of the sound during the largest eruptive bursts was fairly broadband, with energy extending up to ~1500 Hz and the highest amplitudes between 10 and 50 Hz (Figure 14). For example, the frequency of the maximum amplitude within each burst was generally near 12 Hz (Figure 15). At the low-frequency end, the largest bursts were at least 50 dB louder than the quiet intervals between them (the ambient noise), and were ~10 dB louder at 1000 Hz (Figure 14). The spikes in the lower curves in Figure 14 are due to known sources of electronic noise in the hydrophone. There is a notable absence of harmonic tremor, which is a narrow-band signal that typically exhibits a low-frequency fundamental between 1 and 5 Hz with higher frequency harmonics [*McNutt*, 2000]. One reason for the lack of harmonic tremor may be that such low-frequency signals require physically large sources as resonators and that the near-surface volcanic conduit and vent at NW Rota-1 are relatively small. The lack of harmonic tremor is not simply an instrumental artifact, because the B-Probe hydrophone is capable of detecting signals in the 1–10 Hz frequency range, despite its lower-sensitivity due to its high-pass filters. Our interpretation is that the signals recorded by the hydrophone originated at the eruptive vent, rather than at depth in the subseafloor conduit system. Thus, these measurements are somewhat similar to infrasound recordings at volcanoes on land, which are also generated by explosive outflux of magmatic gases [*Johnson*, 2003; *Johnson et al.*, 2003, 2004].

[37] The structure of an individual eruptive burst near the peak in eruptive activity can be characterized by comparing

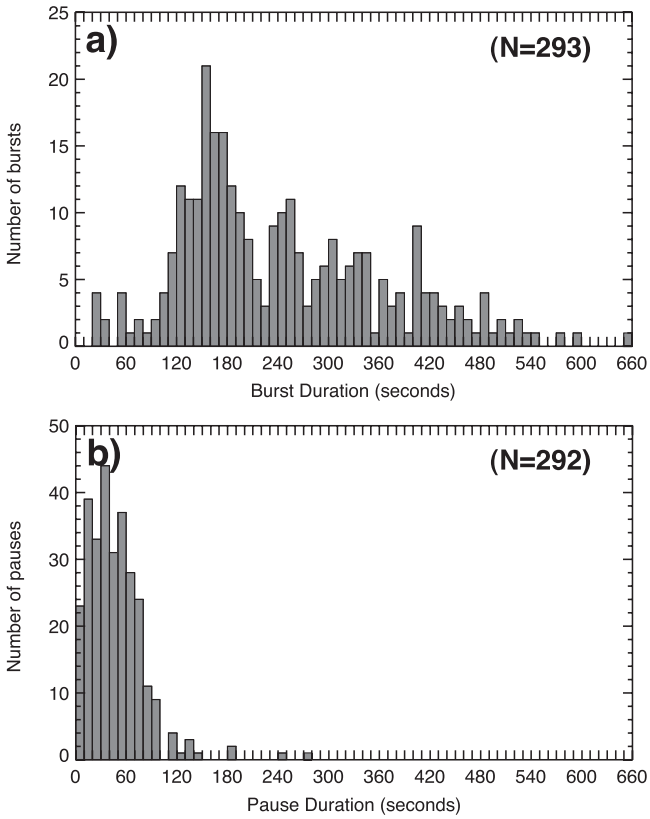

Figure 11. Histograms of the durations of (a) explosive bursts and (b) noneruptive pauses during the second hydrophone deployment. Pauses greater than 100 s were all before 1100 UT on 27 April.

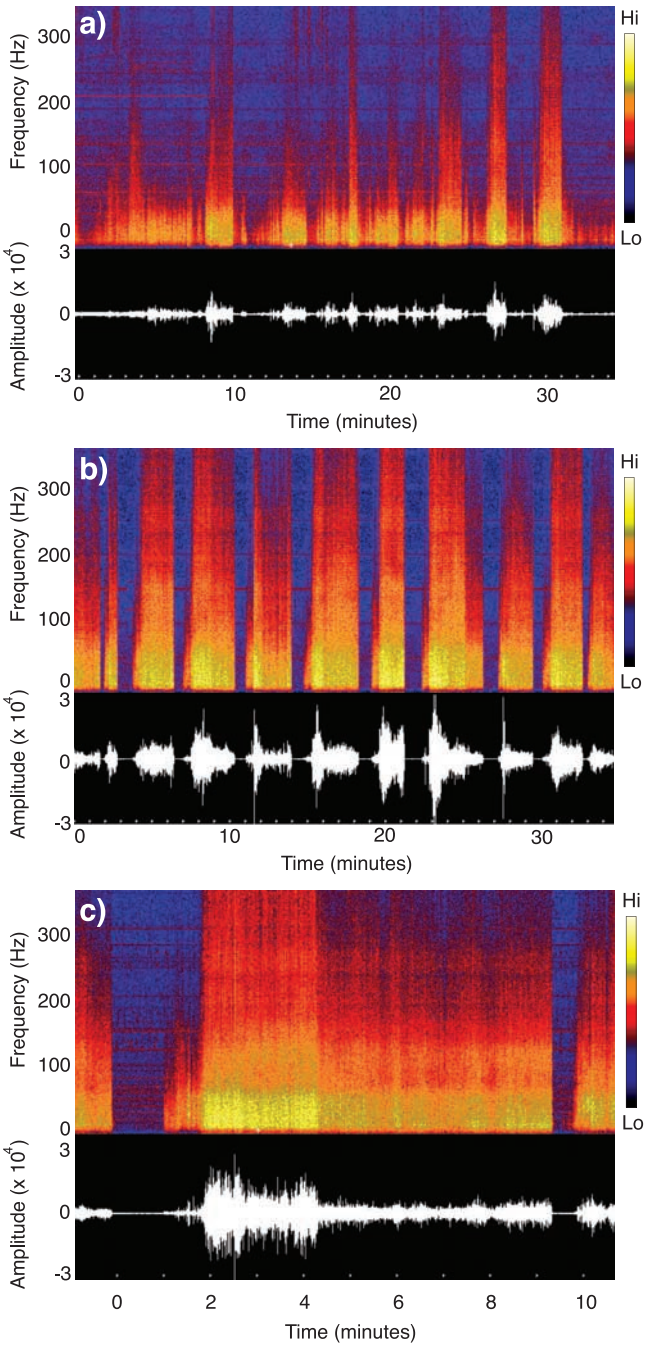

Figure 12. Hydrophone data displayed as both a time series (in digital units, bottom) and spectrogram (in frequency, top), contrasting (a) the early part of the second hydrophone deployment (0346–0420 UT), when the activity was lower and more continuous, with (b) the later part of the record (1300–1334 UT), when eruptive bursts were larger and more discrete. (c) A shorter time series showing the largest eruptive burst observed during the seventh ROV visit to the vent (2056–2108 UT; see also Figures 9e, 9f, and 17 and Movies 14 and 15). At the beginning of a burst, acoustic amplitude gradually built for ~30 s and then suddenly increased when a solidified lava plug in the vent was destroyed. This higher amplitude was usually sustained until the burst abruptly ended.

the acoustic data with ROV video recorded at the same time (Figure 12c). At the start of each acoustic burst there was a sudden onset, followed by a gradual rise in acoustic amplitude for ~30 s, after which the amplitude sharply increased. This higher amplitude was often sustained for the duration of the burst, or in some cases decreased once or twice in discrete steps. From the video observations, the acoustic onset corresponds to a change from passive degassing during a pause to the surge in gas output that started the ejection of pyroclasts. The sharp increase in acoustic amplitude after the first ~30 s marked the appearance and explosive disintegration of a lava plug in the vent, after which the eruptive vigor intensified. The abrupt acoustic shut-off occurred when explosive activity ceased at the vent (Movie 12). The largest explosive event we observed during the seventh visit to Brimstone Pit (the one with the strongest flashes of red glow in the vent) had the same basic structure, but for several minutes right after the lava plug was destroyed had a particularly large acoustic amplitude (Figure 12c). In fact, this same burst had the highest acoustic amplitude measured during any of our observation periods (Figure 16 and Movie 14). This illustrates another key link between the ROV video and hydrophone data: the acoustic

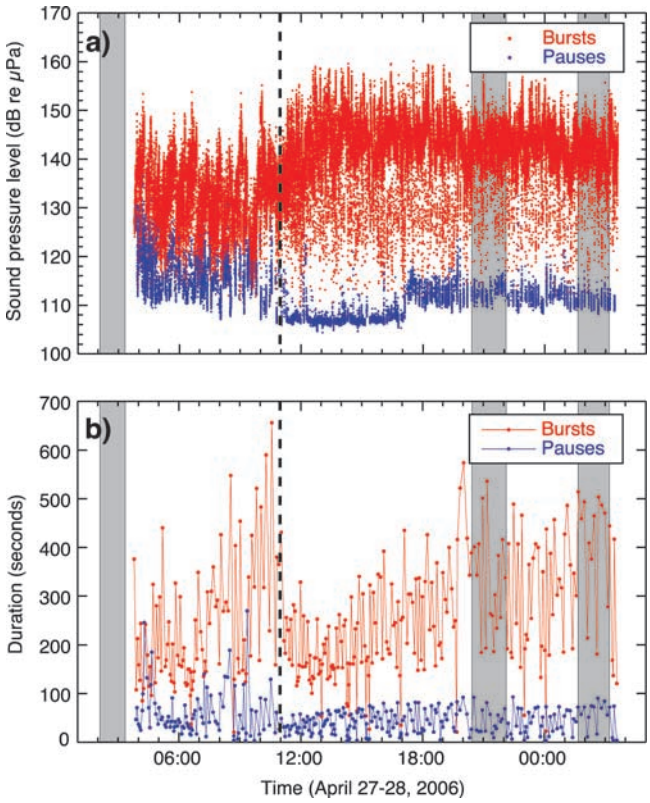

Figure 13. Plots showing a change in character of the eruptive bursts during the second hydrophone deployment. (a) Sound pressure level recorded at the hydrophone averaged every second. Data omitted within ±5 s of transitions between bursts and pauses for clarity. Note change at ~1100 UT on 27 April (vertical dashed line). (b) Duration of the bursts (red) and pauses (blue) plotted versus time. Grey bars show times of sixth, seventh, and eighth ROV visits to the vent.

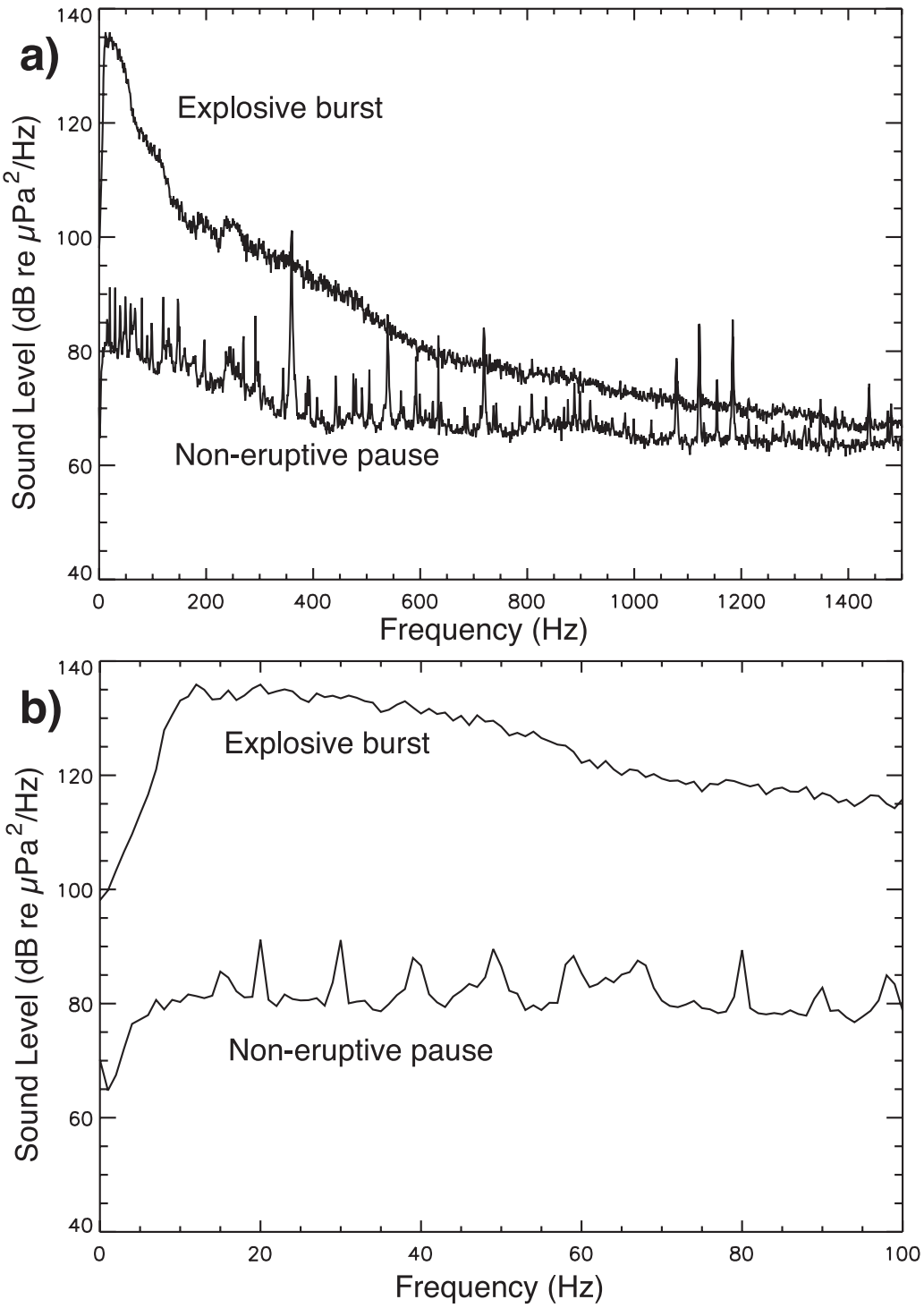

Figure 14. Frequency spectra of the hydrophone data during an eruptive burst (upper curves) versus a noneruptive pause (lower curves). The spectra were created from 1-min samples at 2058:45 UT (upper curves) and 2056:50 UT (lower curves) on 27 April. They are uncorrected for distance from the vent (∼60 m). (a) The largest bursts were broadband with energy up to ∼1500 Hz and were at least 50 dB higher than the ambient noise below 50 Hz. (b) Below 100 Hz, the highest amplitudes are at ∼12 Hz. The spikes in the lower curves are known sources of electronic noise in the B-Probe hydrophone.

amplitude appears directly related to the vigor of the observed explosive activity at the vent. Knowing this, we can use the hydrophone record to infer eruptive activity at the vent when the ROV was not present. For example, the record suggests that the largest explosive events occurred between the sixth and seventh visits when the ROV was not at the vent (Figure 10b). These ''unseen'' bursts were similar in character to those that were witnessed but have

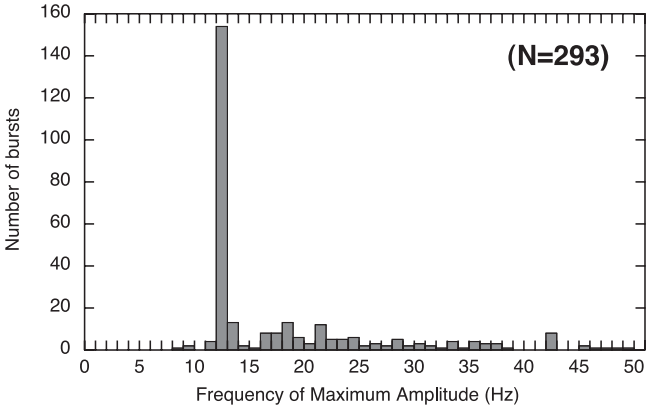

Figure 15. Histogram of the frequency of the maximum acoustic amplitude recorded during each of the 293 eruptive bursts during the second hydrophone deployment.

acoustic amplitudes up to 30% higher, suggesting they were more intense explosions than the ones we observed.

5. Discussion

5.1. A Model for the Explosive Activity at NW Rota-1

[38] We interpret the volcanic activity observed at NW Rota-1 to be submarine Strombolian in eruptive style. Strombolian eruptions are characterized by two-phase flow (in which gas exists as a separate phase from the melt), a low mass eruption rate, a much higher gas flow rate, and episodic explosions [*Vergniolle and Mangan*, 2000]. The eruption rate at Brimstone Pit over the week of observations increased from near zero to 10–100 m^3/h as the activity evolved from slow extrusion to strong explosions (Figure 4); densities of ejecta samples are provided by N. D. Deardorff et al. (manuscript in preparation, 2008). Even at its peak, this eruption rate is relatively low and is within the range of Strombolian eruptions on land [*Vergniolle and Mangan*, 2000]. From an observational perspective, the explosive bursts at Brimstone Pit also appear Strombolian because they are primarily driven by magmatic gases and the explosions are clearly cyclic, which suggests at least partial segregation of gas within the conduit.

[39] To construct an interpretive model for the explosive activity at NW Rota-1, we have looked to the fluid mechanics literature that describes the behavior of buoyancy-driven gas flow in a vertical pipe, in which the fluid medium is static [*Lucas et al.*, 2005; *Mudde*, 2005]. Such an analog is appropriate for NW Rota-1 because the eruption rate is so low that the magma column is essentially static; most of the solid ejecta are simply entrained by the escaping gases. Under these conditions, as the gas flow rate increases, bubbles coalesce and segregate into isolated "slugs" (or "Taylor bubbles") of gas (Figure 17). However, there is also a wide transitional regime between "bubbly flow" at one extreme and "slug flow" at the other [*Lucas et al.*, 2005]. Traditionally, terrestrial Strombolian eruptions have been viewed as fully developed slug flow. That is, they are thought to result from bursting of individual large bubbles of magmatic gas that have coalesced and risen to the top of the volcanic conduit [*Blackburn et al.*, 1976; *Vergniolle and Brandeis*, 1996; *Ripepe et al.*, 2001]. This is manifest at Stromboli volcano with explosions that are typically very brief (1–30 s) and are separated by longer repose intervals of ~12–20 min [*Vergniolle and Mangan*, 2000]. At NW Rota-1, however, the explosions we observed were more sustained (~2–6 min) and had shorter repose intervals (~10–100 s). This suggests to us that the eruptive activity at NW Rota-1 is not fully developed slug flow, but rather a transitional regime between bubbly flow and slug flow (Figure 18). In other words, the magma column at NW Rota-1 is almost static and exsolving magmatic gases are rising as bubbles in the conduit. As these bubbles interact and partially coalesce, they form gas-rich and gas-poor zones, but there is insufficient time and distance along the conduit to form large individual bubbles, as at Stromboli.

[40] In this transitional regime, the behavior of the system is very sensitive to the gas flow rate [*Lucas et al.*, 2005]. We interpret the change in character of the eruptive bursts that occurred at ~1100 UT on 27 April during the second hydrophone record (Figure 13) to reflect an increase in gas flow rate that pushed the system slightly further away from the bubbly flow regime and closer toward the slug flow end of the spectrum. This was evident as a change to more discrete, higher-amplitude explosive bursts, probably because the magmatic gases in the conduit could become more segregated from the melt at a higher gas flow rate.

[41] In this view, each eruptive burst is a bubbly gas-rich pocket reaching the vent, and each noneruptive pause is a (smaller) gas-poor pocket. Passive degassing between bursts allows seawater to penetrate a few meters below the seafloor to the top of the magma column, forming a quenched cap (Figure 18a). When the next gas-rich pocket arrives at the top of the conduit, it immediately starts to force its way through cracks in this cap (Figure 18b). After about 30 s, as the gas pressure builds below the plug, the entire cap is forced upward in the vent and blown apart by violently expanding gases (Figure 18c). The rapidly expanding gas has sufficient velocity to entrain and transport clots of molten and partially vesicular magma (Figure 18d). An explosive burst ends

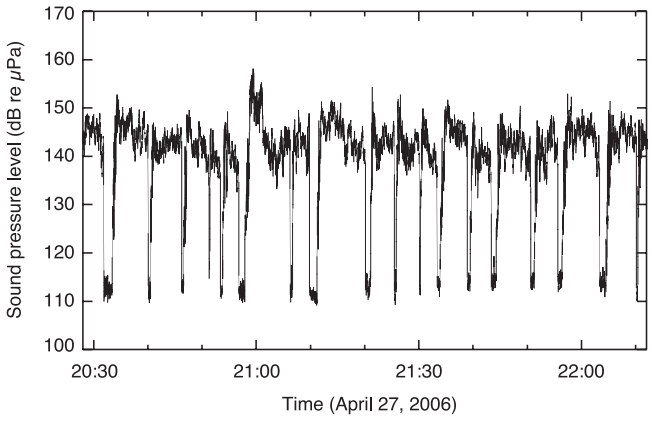

Figure 16. Sound pressure level recorded at the hydrophone (calculated every second) during the seventh ROV visit to Brimstone Pit (2028–2212 UT). Sounds between 130 and 160 dB are the eruptive bursts; sounds between 110 and 120 dB are the noneruptive pauses. The burst with the highest amplitude during this time interval (~2100) was accompanied by flashes of red glow in the vent; see also Figures 9e, 9f, 12c, and 14 and Movies 14 and 15.

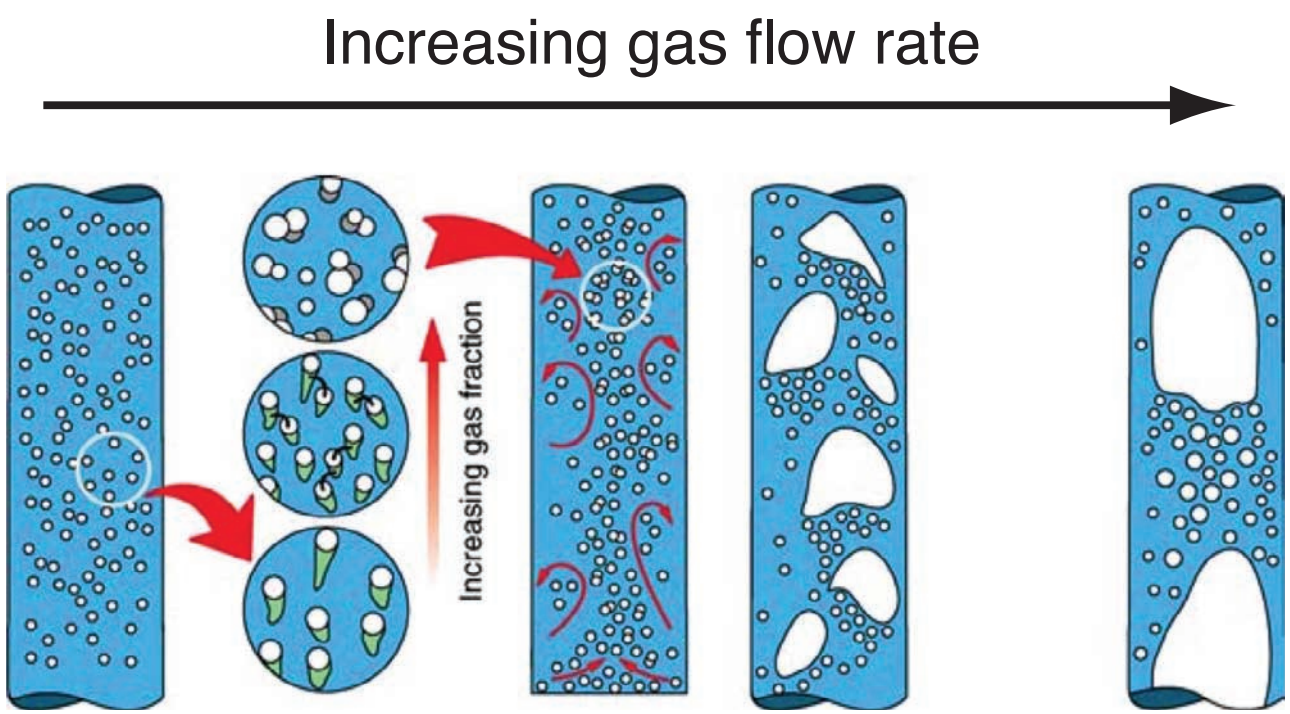

Figure 17. Illustration showing that buoyancy-driven gas flow (white) in a vertical pipe filled with liquid (blue) that is static, evolves from bubbly flow to slug flow with increasing gas flow rate [from *Mudde*, 2005].

when the last of the gas-rich pocket is vented and the system returns to the rest state whereupon another cap will begin to form. The cycle is repeated when the next pocket of gas arrives at the vent. This model is supported by the positive correlation between the duration of each pause and the duration of the following burst (Figure 19). This suggests that the gas flow rate is more or less steady, and the longer it has been since the last burst, the more gas will accumulate below the cap, and hence the longer the next burst will be.

5.2. Magma-Seawater Interaction at NW-Rota-1

[42] Given that the eruptions appear to be driven primarily by magmatic gases, we can now ask what role, if any, seawater played in creating the explosive activity? The effect of seawater interaction is most apparent during the most intense explosive bursts observed late in the dive series, when rapid oscillations in the vent were accompanied by flashes of red glow in the core of the eruption plume. We suggest that these two observations are linked – that exposure of molten lava to seawater during high-intensity activity allows seawater to momentarily flash to steam, causing plume expansion, before cooling and condensing an instant later, causing plume contraction. This process occurs repeatedly, many times per second, to cause the rapid oscillations observed in the vent during the peak in activity. Steam generated in this manner is necessarily short-lived, as there is no mechanism to keep the vapor in contact with the hot lava. Instead, the steam mixes quickly with seawater, cools and condenses, and the surface of the lava is quenched. The next discharge of hot lava erupted from the vent then repeats and continues the process that produced the oscillations.

[43] The audible sound that was recorded during these bursts by the hydrophone has a vibrating or pulsating quality (Movie 14). Indeed, the plume oscillations visible in the video occur at about the same rate as the fundamental frequency peak in the hydrophone data recorded at the same time. Frame-by-frame examination of the video during selected 1-s time intervals shows that expansion and contraction of the core of the eruption plume occurs at frequencies of 5–10 Hz (Table 3). During these same 1-s intervals, the number of dominant peaks in the acoustic time series and the lowest peak in the frequency spectra (the "fundamental") were similar (Figures 20a and 20b). Overtones (integer multiples of the fundamental frequency) in the spectra are harmonic resonances related to the fundamental (the lowest frequency peak) and often have higher amplitude (Figures 20a and 20b), but this is partially because of the hydrophone's high-pass filters. The exact time series and distribution of frequency peaks vary depending on the 1-s time interval chosen, but the frequency of the maximum acoustic amplitude during each burst (measured over its entire duration) is almost always ~12 Hz (Figure 15).

[44] Another measure of the characteristic frequency of magma-seawater interaction during periods of high-intensity eruption is the number of video frames of selected 1-s time intervals in which red glow is visible at the vent. This measure is not ideal because glow may be visible for multiple frames in a row and at other times it may be masked by the surrounding plume. Nevertheless, when the visibility at the vent was good a red glow was visible in 10–19 frames out of 30 in each 1-s interval, most often around 12 frames/s (Table 3). The acoustic data recorded at the same time also shows a peak at ~12 Hz (Figures 20c and 20d). Therefore, it appears that oscillating formation and condensation of steam may also contribute to the hydrophone sound recorded during the eruptive bursts. This oscillating steam formation was the only type of explosive interaction between magma and seawater observed at NW Rota-1.

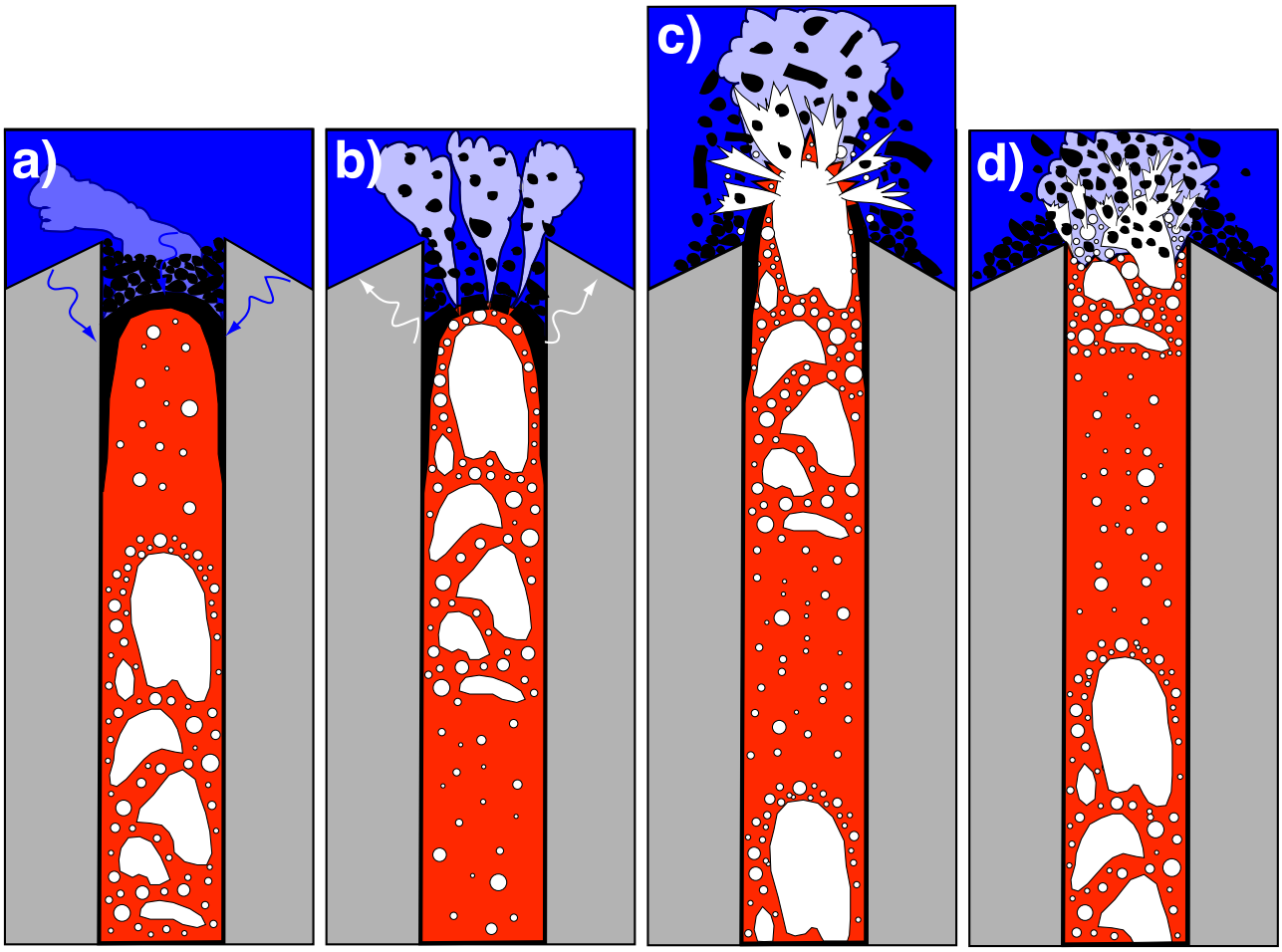

Figure 18. Model for the eruptive activity observed at NW Rota-1 in 2006 (red, magma; white, magmatic gases; blue, seawater; black, solidified lava). (a) Between bursts, seawater cools the top of the magma column, forming a solidified cap. (b) When the next gas-rich pocket reaches the cap, it immediately starts to escape. (c) The gas pocket forces the lava cap upward in the vent where explosions destroy it. (d) With the vent uncapped, the eruptive burst proceeds at a higher level until all the gas in the pocket is vented and the activity abruptly ceases, returning to the initial state.

5.3. Comparison to Acoustic Records of Previous Underwater Volcanic Activity

[45] It is well known that bubble formation, and especially vapor collapse, produces significant sound underwater [*Strasberg*, 1956; *Leet*, 1988; *Lu et al.*, 1990; *Yoon et al.*, 1991]. Acoustic measurements made in crater lakes [*Bercy et al.*, 1983; *Vandemeulebrouck et al.*, 1994; *Hurst and Vandemeulebrouck*, 1996; *Vandemeulebrouck et al.*, 2000] and in geyser conduits [*Kieffer*, 1984] where vapor collapse was suspected have recorded sound between 1 and 60 Hz, similar to the peak amplitudes observed at NW Rota-1. Far-field hydroacoustic records of submarine eruptive activity have measured peak energy in this same frequency range, and as high as 1000 Hz during larger events [*Dietz and Sheehy*, 1954; *Snodgrass and Richards*, 1956; *Kibblewhite*, 1966; *Norris and Johnson*, 1969; *Norris and Hart*, 1970; *Talandier and Okal*, 1987; *Talandier*, 1989]. The closest resemblance in temporal character to the activity at NW Rota-1 has been described from Rumble III and Monowai submarine volcanoes, both located in the Kermadec arc. *Kibblewhite* [1966] described a hydroacous-

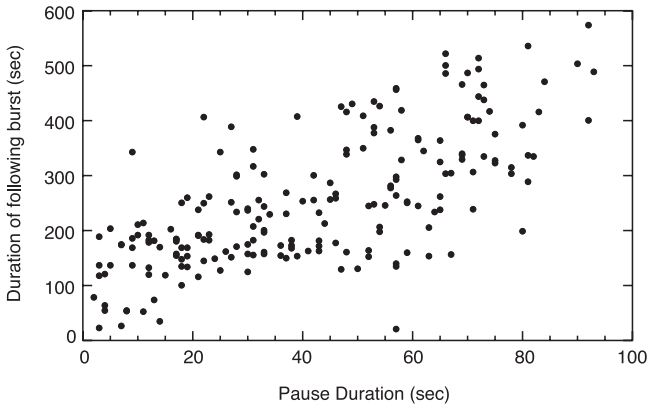

Figure 19. Plot showing the duration of each noneruptive pause versus the duration of the following explosive burst. Only durations after 1100 UT on 27 April are shown when the bursts and pauses were most distinct. The positive correlation suggests that the rate of gas discharge was steady during this time interval, and longer pauses allowed more gas to accumulate before the next burst.

Table 3. Visible Frequency of Plume Oscillation and Red Glow[a]

Plume Oscillation		Red Glow	
Start Time (UT)	Frequency (Hz)	Start Time (UT)	Frequency (Hz)
2059:08	10	2058:52	12
2059:09	9	2058:53	13
2059:10	8	2058:54	10
2145:05	6	2058:55	12
2145:06	8	2059:01	12
2145:07	6	2059:02	14
2145:20	8	2059:03	19
2145:21	6	2059:04	12
2145:22	7	2059:16	10
2145:23	5	2059:19	12
	7.3[b]		12.6[b]

[a]The frequencies listed are the number of times the phenomenon was observed in one second of video (at 30 frames/s) from the start time. All of the above observations were made on Jason dive J2-192 during the seventh visit to Brimstone Pit on 27 April 2006.
[b]Average.

tic source (probably Rumble III seamount [*Wright*, 1994]) that produced cyclic rises and falls of amplitude with a period of ~3–5 min, lasting hours at a time, and persisting for over 8 years. Monowai cone has been a frequent source of T wave swarms during the last 30 years, each commonly lasting several days and consisting of hundreds of individual events, with durations of 5–10 min and highest amplitudes below 5 Hz [*Davey*, 1980; *Wright et al.*, 2008]. These signals are interpreted as magma-seawater reactions in the vent conduit during explosive activity, and have both similarities (rhythmic events with similar durations) and differences (lower frequency content) to the acoustic events at NW Rota-1. However, it is difficult to make direct comparisons, because (as far as we know) none of the eruptive activity at NW Rota-1 between 2004 and 2006 was detected by far-field seismic or hydrophone networks, probably because of the relatively low source amplitudes and acoustic shadowing to the east by the uplifted parts of the Mariana forearc that include the islands of Guam, Rota, and Saipan (Figure 1).

5.4. Comparison to Previous Models of Submarine Eruptions

[46] In this section we place the observations at NW Rota-1 into the context of previous ideas about submarine explosive eruptions at basaltic volcanoes. At issue are both the nature and extent of lava-water interaction during these eruptions, and the role that magmatic volatiles play. *Kokelaar* [1986] describes four primary explosive processes for submarine basaltic volcanoes: (1) magmatic explosivity (driven by rapid expansion of magmatic gases), (2) contact surface steam explosivity (also termed molten fuel-coolant interactions), (3) bulk interaction steam explosivity (from entrapment of water in magma), and (4) cooling-contraction granulation. Within this scheme, we would classify the eruptive activity at NW Rota-1 as driven primarily by "magmatic explosivity," with "contact-surface explosivity" a minor secondary phenomenon in the vent. Contact-surface explosivity occurs when magma in contact with water forms a thin film of steam on the surface. The film can then become unstable, oscillating as it expands and contracts [*Wohletz*, 1986]. Under the right conditions, this "film boiling" process can fragment the melt and vigorously mix it with water, increasing heat transfer, leading to a violently escalating reaction. Experimental results show that for the most explosive interactions the optimal water/magma mass ratio is ~0.35 [*Wohletz*, 1986]. Therefore, the minor role of this process at NW Rota-1 may be due to the very low eruption rate and the high water/magma ratio in the vent, conditions not conducive to sustaining such reactions. Magma/water interactions that actually drive explosive eruptions probably only occur at much shallower depths, during much higher eruption rates, or associated with magma intrusions into water-saturated sediment [*Kokelaar*, 1986; *Clague et al.*, 2003a; *White et al.*, 2003].

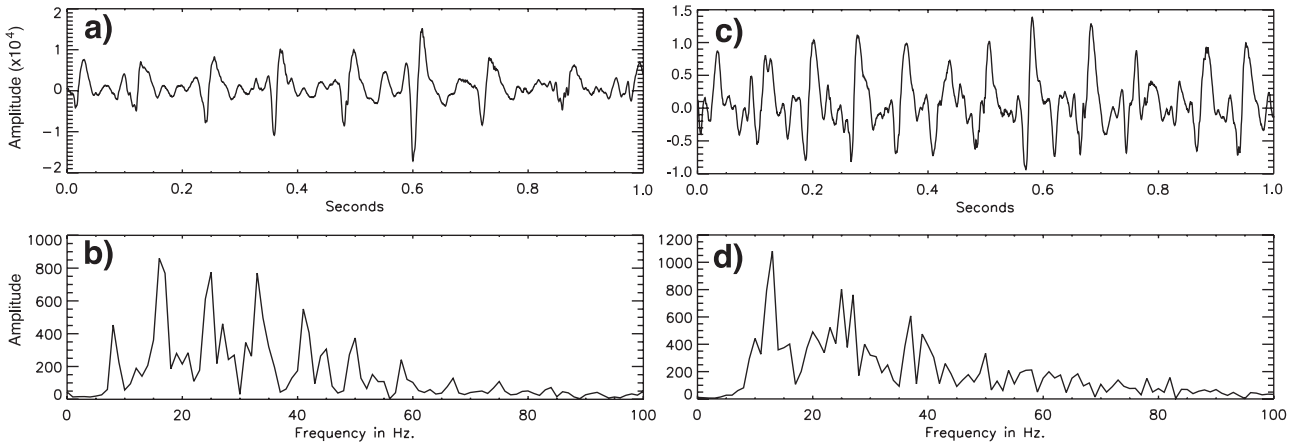

Figure 20. Hydrophone data showing time series and frequency spectra pairs from 1-s time intervals during magma-seawater interaction, manifested as (a and b) plume oscillation (J2-192, 2059:08 UT) and (c and d) flashes of red glow (J2-192, 2059:03 UT). The frequency spectrum in Figure 20b shows a fundamental peak near 9 Hz and higher-amplitude overtones at integer multiples of 9 Hz. The spectrum in Figure 20d has a high-amplitude fundamental peak at 12 Hz and weaker overtones. These are compared with visual observations in Table 3 and Movie 14. Time series amplitudes in Figures 20a and 20c are in digital units.

[47] The depth limit of subaqueous explosive basaltic volcanism was once thought to be only 500–800 m [*McBirney*, 1963; *Fisher and Schmincke*, 1984; *Staudigel and Schmincke*, 1984]. Later, *Kokelaar* [1986] argued that magmatic explosivity could extend well below 1000 m in volcanic arcs because of high volatile contents. Although *Head and Wilson* [2003] did not consider the volcanic arcs, their calculations suggest that pyroclastic activity could be possible to at least 3000 m, although probably much diminished in vigor at those depths. Indeed, a number of studies have documented clear evidence of explosive basaltic eruptions below 1000 m from the morphology of pyroclastic deposits, including on Loihi seamount (<1350 m) [*Clague et al.*, 2003a], the Mid-Atlantic Ridge (<1750 m) [*Fouquet et al.*, 1998; *Eissen et al.*, 2003], the Sumisu back arc (<1800 m) [*Gill et al.*, 1990], the Gorda Ridge (<3850 m) [*Clague et al.*, 2003b], and from the North Arch volcanic field around Hawaii (<4200 m) [*Davis and Clague*, 2006]. As the role of steam explosivity is effectively limited to depths above ~2940 m, where heated seawater reaches its critical point [*Bischoff and Rosenbauer*, 1988], the deepest examples are apparently due to unusually high volatile contents (CO_2 in alkalic basalts; H_2O in arc magmas) or concentrations of volatiles at the top of a magma reservoir in a "magmatic foam" [*Head and Wilson*, 2003; *White et al.*, 2003]. We do not see these kinds of delicate pyroclasts in the NW Rota-1 deposits, because the high H_2O content of the lavas makes them too crystalline (N. D. Deardorff et al., manuscript in preparation, 2008). In any case, the activity at NW Rota-1 clearly shows that explosive eruptions at basaltic arc volcanoes are possible down to at least 560 m. Since the eruption rate at NW Rota-1 was fairly low and was characterized by gas flowing freely up the conduit (suggesting exsolution occurred at depths well below the vent), it seems likely that arc volcanoes could produce vigorous explosive behavior at considerably greater depths with higher mass eruption rates.

[48] Also unknown is the maximum depth from which submarine explosions can reach the ocean's surface. Many examples are known of near-surface explosive activity (Surtsey, Myôjin Reef, MacDonald Seamount, Kavachi, etc.), but there are only four well-documented examples of volcanic explosions breaking the surface from water depths > 100 m [*Mastin and Witter*, 2000]. Physical considerations suggest surface-breaking eruptions should be increasingly improbable below this depth [*Zimanowski and Büttner*, 2003]. At NW Rota-1, the maximum plume height from the witnessed eruptive activity did not extend more than 100 m above the vent. It seems unlikely that the eruptions from NW Rota-1 could reach the surface, even if the eruption rate increased by several orders of magnitude. It is clear that the vertical momentum of erupted pyroclasts decreases very rapidly due to drag in seawater, and thus at higher eruption rates we envision that the primary difference would be an increase in the load of downslope transport of volcaniclastic material, contributing to the vast aprons of such deposits around other Mariana seamounts [*Embley et al.*, 2006b].

6. Conclusions

[49] Submarine explosive activity was witnessed at NW Rota-1 volcano in the Mariana arc three times in 2 years, suggesting that the volcano is in a period of long-term, possibly continuous activity characterized by repeated buildup and collapse of a cinder cone over the active vent area known as Brimstone Pit. This interpretation is supported by the fact that the volume of depth change between bathymetric surveys in 2003 and 2006 (3.3×10^7 m^3) is consistent with the volcano being continuously active during that time at the eruption rate that we observed in 2006 (10–100 m^3/h) [*Walker et al.*, 2008].

[50] Over the week of observations in 2006 we saw a transition from nonexplosive extrusion to explosive eruptions as the eruption rate increased by at least an order of magnitude. However, we interpret that the rate of magmatic gas release controlled the activity we observed, such that as the gas flux increased more magma was simply entrained and erupted. The landslide/eruptive event that just preceded our dive series at NW Rota-1 in 2006 may have been a major exhalation of the magmatic system, from which the volcano was recovering when we arrived. The data from a portable hydrophone deployed near the vent support the interpretation that the variation in eruptive style we observed was caused by an increasing gas flux, and we speculate that the acoustic amplitude data are a good proxy for gas flow rate. Our observations can be interpreted in terms of the physics of buoyancy-driven bubbly flow in a vertical pipe, and we view the activity at NW Rota-1 as transitional between bubbly flow and fully developed slug flow. The eruptive style at NW Rota-1 is interpreted to be submarine Strombolian, in which episodic explosions are driven by partially segregated pockets of magmatic gas rising in the volcanic conduit.

[51] Our observations of activity in April 2006 are unique in several ways, and provide important insight into processes active in submarine and subaerial arc environments. We were able to view the eruptive activity at extremely close range, and the underwater setting allowed extraordinary visualization of magmatic degassing processes. We interpret that magmatic H_2O was the primary driver of the short-lived explosive bursts, while CO_2 dominated gas release appeared to be passive, both preceding explosions and rising from explosive bursts as clear gas bubbles. Sulfur gases were also released syneruptively, but as billowing cloudy plumes full of tiny molten droplets that eventually cooled to solidified beads and fell to the seafloor. This interpretation is based on our video observations that show that the different gas phases have strikingly different behavior, that H_2O is the dominant volatile at NW Rota-1 (as is typical for arc volcanoes) [*Wallace and Anderson*, 2000; *Shaw et al.*, 2006], and that H_2O has the highest potential for volumetric expansion at magmatic temperatures [*Keenan et al.*, 1969; *Perfit et al.*, 2003]. In contrast, magma/seawater interaction was rather minimal under these eruption conditions.

[52] **Acknowledgments.** The observations reported here were part of the Submarine Ring of Fire Project sponsored by the NOAA Ocean Exploration and NOAA Vents Programs. This work was made possible by the outstanding support from the captain and crew of the R/V *Melville*, operated by the Scripps Institution of Oceanography, and the crew of the *Jason* ROV, operated by the Woods Hole Oceanographic Institution. Will Sellers was the *Jason* Expedition Leader. Bill Burgess of Greeneridge Sciences provided help and advice with the B-Probe hydrophone, which was developed with support from the Office of Naval Research. Dan Scheirer wrote the software used to process the Imagenex scanning sonar data. Sharon Nieukirk and Dave Mellinger provided help with acoustic visual-

ization software. K.V.C. acknowledges funding from NSF EAR0510493 for support for this work. Detailed and very helpful reviews by David Clague and Jeffrey Johnson greatly improved the manuscript. PMEL contribution 3078.

References

Baker, E. T., R. Embley, S. L. Walker, J. A. Resing, J. Lupton, K. Nakamura, C. E. J. de Ronde, and G. Massoth (2008), Hydrothermal activity and volcano distribution along the Mariana arc, *J. Geophys. Res.*, doi:10.1029/2007JB005423, in press.

Bercy, C., J.-C. Sabroux, and G. Suparwoto (1983), Underwater noise survey in the crater lake of Kelut volcano (Indonesia), in *Forecasting Volcanic Events*, edited by H. Tazieff and J.-C. Sabroux, pp. 529–543, Elsevier, Amsterdam, Netherlands.

Bischoff, J. L., and R. J. Rosenbauer (1988), An empirical equation of state for hydrothermal seawater, *Am. J. Sci.*, *285*, 725–763.

Blackburn, E. A., L. Wilson, and R. S. J. Sparks (1976), Mechanisms and dynamics of Strombolian activity, *J. Geol. Soc.*, *132*, 429–440, doi:10.1144/gsjgs.132.4.0429.

Bloomer, S. H., R. J. Stern, and N. C. Smoot (1989), Physical volcanology of the submarine Mariana and volcano arcs, *Bull. Volcanol.*, *51*, 210–224, doi:10.1007/BF01067957.

Butterfield, D. A., R. W. Embley, W. W. Chadwick, Jr., J. E. Lupton, K. Nakamura, B. Takano, C. E. J. de Ronde, J. Resing, S. Bolton, and J. Baross (2006), Up-close fluid sampling at a deep submarine lava eruption, *Eos Trans. AGU*, *87*(52), Fall Meet. Suppl., Abstract V13C-07.

Chadwick, W. W., Jr., D. S. Scheirer, R. W. Embley, and H. P. Johnson (2001), High-resolution bathymetric surveys using scanning sonars: Lava flow morphology, hydrothermal vents and geologic structure at recent eruption sites on the Juan de Fuca Ridge, *J. Geophys. Res.*, *106*(B8), 16,075–16,100, doi:10.1029/2001JB000297.

Clague, D. A., R. Batiza, J. W. Head III, and A. S. Davis (2003a), Pyroclastic and hydroclastic deposits on Loihi Seamount, Hawaii, in *Explosive Subaqueous Volcanism*, *Geophys. Monogr. Ser.*, vol. 140, edited by J. D. L. White et al., pp. 73–96, AGU, Washington, D. C.

Clague, D. A., A. S. Davis, and J. E. Dixon (2003b), Submarine Strombolian eruptions on the Gorda mid-ocean ridge, in *Explosive Subaqueous Volcanism*, *Geophys. Monogr. Ser.*, vol. 140, edited by J. D. L. White et al., pp. 111–128, AGU, Washington, D. C.

Davey, F. J. (1980), The Monowai seamount: An active submarine volcanic centre on the Tonga-Kermadec ridge, *N. Z. J. Geol. Geophys.*, *23*, 533–536.

Davis, A. S., and D. A. Clague (2006), Volcaniclastic deposits from the North Arch volcanic field, Hawaii: Explosive fragmentation of alkalic lava at abyssal depths, *Bull. Volcanol.*, *68*, 294–307, doi:10.1007/s00445-005-0008-7.

de Ronde, C. E. J., et al. (2005), Evolution of a submarine magmatic-hydrothermal system: Brothers volcano, southern Kermadec arc, New Zealand, *Econ. Geol.*, *100*, 1097–1133, doi:10.2113/100.6.1097.

Dietz, R. S., and M. J. Sheehy (1954), Transpacific detection of Myôjin volcanic explosions by underwater sound, *Geol. Soc. Am. Bull.*, *65*, 941–956, doi:10.1130/0016-7606(1954)65[941:TDOMVE]2.0.CO;2.

Eissen, J.-P., Y. Fouquet, D. Hardy, and H. Ondréas (2003), Recent MORB volcaniclastic explosive deposits formed between 500 and 1750 m.b.s.l. on the axis of the Mid-Atlantic Ridge, south of the Azores, in *Explosive Subaqueous Volcanism*, *Geophys. Monogr. Ser.*, vol. 140, edited by J. D. L. White et al., pp. 143–166, AGU, Washington, D. C.

Embley, R. W., E. T. Baker, W. W. Chadwick Jr., J. E. Lupton, J. A. Resing, G. J. Massoth, and K. Nakamura (2004), Explorations of Mariana arc volcanoes reveal new hydrothermal systems, *Eos Trans. AGU*, *85*(4), 3740.

Embley, R. W., et al. (2006a), Long-term eruptive activity at a submarine arc volcano, *Nature*, *441*, 494–497, doi:10.1038/nature04762.

Embley, R. W., W. W. Chadwick Jr., R. J. Stern, S. G. Merle, S. H. Bloomer, K. Nakamura, and Y. Tamura (2006b), A synthesis of multibeam bathymetry and backscatter, and sidescan sonar of the Mariana submarine magmatic arc, western Pacific, *Eos Trans. AGU*, *87*(52), Fall Meet. Suppl., Abstract V41B-1723.

Fisher, R. V., and H.-U. Schmincke (1984), *Pyroclastic Rocks*, 472 pp., Springer, Berlin, Germany.

Fouquet, Y., J.-P. Eissen, H. Ondréas, F. Barriga, R. Batiza, and L. Danyushevsky (1998), Extensive volcaniclastic deposits at the Mid-Atlantic Ridge axis: Results of deep-water basaltic explosive activity, *Terra Nova*, *10*, 280–286, doi:10.1046/j.1365-3121.1998.00204.x.

Gill, J., et al. (1990), Explosive deep water basalt in the Sumisu backarc rift, *Science*, *248*, 1214–1217, doi:10.1126/science.248.4960.1214.

Gregg, T. K. P., and D. J. Fornari (1998), Long submarine lava flows: Observations and results from numerical modeling, *J. Geophys. Res.*, *103*(B11), 27,517–27,532, doi:10.1029/98JB02465.

Griffiths, R. W., and J. H. Fink (1992), Solidification and morphology of submarine lavas: A dependence on extrusion rate, *J. Geophys. Res.*, *97*(B13), 19,729–19,737, doi:10.1029/92JB01594.

Head, J. W., and L. Wilson (2003), Deep submarine pyroclastic eruptions: Theory and predicted landforms and deposits, *J. Volcanol. Geotherm. Res.*, *121*, 155–193, doi:10.1016/S0377-0273(02)00425-0.

Hurst, A. W., and J. Vandemeulebrouck (1996), Acoustic noise and temperature monitoring of the crater lake of Mount Ruapehu volcano, *J. Volcanol. Geotherm. Res.*, *71*, 45–51, doi:10.1016/0377-0273(95)00060-7.

Johnson, J. B. (2003), Generation and propagation of infrasonic airwaves from volcanic explosions, *J. Volcanol. Geotherm. Res.*, *121*, 1–14, doi:10.1016/S0377-0273(02)00408-0.

Johnson, J. B., R. C. Aster, M. C. Ruiz, S. D. Malone, P. J. McChesney, J. M. Lees, and P. R. Kyle (2003), Interpretation and utility of infrasonic records from erupting volcanoes, *J. Volcanol. Geotherm. Res.*, *121*, 15–63, doi:10.1016/S0377-0273(02)00409-2.

Johnson, J. B., R. C. Aster, and P. R. Kyle (2004), Volcanic eruptions observed with infrasound, *Geophys. Res. Lett.*, *31*, L14604, doi:10.1029/2004GL020020.

Keenan, J. H., F. G. Keyes, P. G. Hill, and J. G. Moore (1969), *Steam Tables: Thermodynamic Properties of Water Including Vapor, Liquid, and Solid Phases*, 162 pp., John Wiley, New York.

Kibblewhite, A. C. (1966), The acoustic detection and location of an underwater volcano, *N. Z. J. Sci.*, *9*(1), 178–199.

Kieffer, S. W. (1984), Seismicity at Old Faithful geyser: An isolated source of geothermal noise and possible analogue of volcanic seismicity, *J. Volcanol. Geotherm. Res.*, *22*, 59–95, doi:10.1016/0377-0273(84)90035-0.

Kokelaar, B. P. (1986), Magma-water interactions in subaqueous and emergent basaltic volcanism, *Bull. Volcanol.*, *48*, 275–289, doi:10.1007/BF01081756.

Leet, R. C. (1988), Saturated and subcooled hydrothermal boiling in groundwater flow channels as a source of harmonic tremor, *J. Geophys. Res.*, *93*(B5), 4835–4849, doi:10.1029/JB093iB05p04835.

Lu, N. Q., A. Prosperetti, and S. W. Yoon (1990), Underwater noise emissions form bubble clouds, *IEEE J. Oceanic Eng.*, *15*(4), 275–281, doi:10.1109/48.103521.

Lucas, D., E. Krepper, and H.-M. Prasser (2005), Development of co-current air-water flow in a vertical pipe, *Int. J. Multiphase Flow*, *31*, 1304–1328, doi:10.1016/j.ijmultiphaseflow.2005.07.004.

Mastin, L. G., and J. B. Witter (2000), The hazards of eruptions through lakes and seawater, *J. Volcanol. Geotherm. Res.*, *97*, 195–214, doi:10.1016/S0377-0273(99)00174-2.

McBirney, A. R. (1963), Factors governing the nature of submarine volcanism, *Bull. Volcanol.*, *26*, 455–469, doi:10.1007/BF02597304.

McNutt, S. R. (2000), Volcanic seismicity, in *Encyclopedia of Volcanoes*, edited by H. Sigurdsson, pp. 1015–1033, Academic, San Diego, Calif.

Mudde, R. F. (2005), Gravity driven bubbly flows, *Annu. Rev. Fluid Mech.*, *37*, 393–423, doi:10.1146/annurev.fluid.37.061903.175803.

Norris, R. A., and D. N. Hart (1970), Confirmation of sofar-hydrophone detection of submarine eruptions, *J. Geophys. Res.*, *75*(11), 2144–2147, doi:10.1029/JB075i011p02144.

Norris, R. A., and R. H. Johnson (1969), Submarine volcanic eruptions recently located in the Pacific by Sofar hydrophones, *J. Geophys. Res.*, *74*(2), 650–664, doi:10.1029/JB074i002p00650.

Perfit, M. R., J. R. Cann, D. J. Fornari, J. L. Engels, D. K. Smith, W. I. Ridley, and M. H. Edwards (2003), Interaction of sea water and lava during submarine eruptions at mid-ocean ridges, *Nature*, *426*, 62–65, doi:10.1038/nature02032.

Resing, J. A., G. Lebon, E. T. Baker, J. E. Lupton, R. W. Embley, G. J. Massoth, W. W. Chadwick Jr., and C. E. J. de Ronde (2008), Venting of acid-sulfate fluids in a high-sulfidation setting at NW Rota-1 submarine volcano on the Mariana Arc, *Econ. Geol.*, *102*, 1047–1061.

Ripepe, M., S. Ciliberto, and M. D. Schiava (2001), Time constraints for modeling source dynamics of volcanic explosions at Stromboli, *J. Geophys. Res.*, *106*(B5), 8713–8727, doi:10.1029/2000JB900374.

Shaw, A. M., E. Hauri, Y. Tamura, O. Ishizuka, R. J. Stern, and R. W. Embley (2006), Volatile contents of NW Rota melt inclusions: Insight to explosive submarine arc volcanism, *Eos Trans. AGU*, *87*(52), Fall Meet. Suppl., Abstract V52B-05.

Snodgrass, J. M., and A. F. Richards (1956), Observations of underwater volcanic acoustics at Bárcena volcano, San Benedicto Island, Mexico, and in Shelikof Strait, Alaska, *Eos Trans. AGU*, *37*(1), 97–104.

Staudigel, H., and H.-U. Schmincke (1984), The Pliocene seamount series of La Palma/Canary Islands, *J. Geophys. Res.*, *89*(B13), 11,195–11,215, doi:10.1029/JB089iB13p11195.

Stern, R. J., M. J. Fouch, and S. L. Klemperer (2003), An overview of the Izu-Bonin-Mariana subduction factory, in *Inside the Subduction Factory*,

Geophys. Monogr. Ser., vol. 138, edited by J. Eiler, pp. 175–222, AGU, Washington, D. C., doi:10.1029/1138GM1010.

Strasberg, M. (1956), Gas bubbles as sources of sound in liquids, *J. Acoust. Soc. Am.*, *28*(1), 20–26, doi:10.1121/1.1908212.

Talandier, J. (1989), Submarine volcanic activity: Detection, monitoring, and interpretation, *Eos Trans. AGU*, *70*(18), 561, 568–569.

Talandier, J., and E. A. Okal (1987), Seismic detection of underwater volcanism: The example of French Polynesia, *Pure Appl. Geophys.*, *125*, 919–950, doi:10.1007/BF00879361.

Tamura, Y., O. Ishizuka, A. M. Shaw, R. J. Stern, R. W. Embley, H. Kawabata, H. Shukuno, K. Tani, and Q. Chang (2006), Torishima and NW Rota-1: A petrological contrast between the Izu-Bonin and Mariana arcs, *Eos Trans. AGU*, *87*(52), Fall Meet. Suppl., Abstract V51F-07.

Vandemeulebrouck, J., A. W. Hurst, and N. Poussielgue (1994), Implications for the thermal regime of acoustic noise measurements in Crater Lake, Mount Ruapehu, New Zealand, *Bull. Volcanol.*, *56*, 493–501, doi:10.1007/BF00302830.

Vandemeulebrouck, J., J.-C. Sabroux, M. Halbwachs, Surono, N. Poussielgue, J. Grangeon, and J. Tabbagh (2000), Hydroacoustic noise precursors of the 1990 eruption of Kelut volcano, Indonesia, *J. Volcanol. Geotherm. Res.*, *97*, 443–456, doi:10.1016/S0377-0273(99)00176-6.

Vergniolle, S., and G. Brandeis (1996), Strombolian explosions: 1. A large bubble breaking at the surface of a lava column as a source of sound, *J. Geophys. Res.*, *101*(B9), 20,433–20,448, doi:10.1029/96JB01178.

Vergniolle, S., and M. T. Mangan (2000), Hawaiian and Strombolian eruptions, in *Encyclopedia of Volcanoes*, edited by H. Sigurdsson, pp. 447–461, Academic, San Diego, Calif.

Walker, S. L., E. T. Baker, G. T. Lebon, J. A. Resing, and J. E. Lupton (2008), Eruption-fed particle plumes at a submarine volcano: NW-Rota-1, Mariana Arc, *J. Geophys. Res.*, doi:10.1029/2007JB005441, in press.

Wallace, P., and A. T. Anderson Jr. (2000), Volatiles in magmas, in *Encyclopedia of Volcanoes*, edited by H. Sigurdsson, pp. 149–170, Academic, San Diego, Calif.

White, J. D. L., J. L. Smellie, and D. A. Clague (2003), Introduction: A deductive outline and topical overview of subaqueous explosive volcanism, in *Explosive Subaqueous Volcanism*, *Geophys. Monogr. Ser.*, vol. 140, edited by J. D. L. White et al., pp. 1–23, AGU, Washington, D. C.

Wohletz, K. H. (1986), Explosive magma-water interactions: Thermodynamics, explosion mechanisms, and field studies, *Bull. Volcanol.*, *48*, 245–264, doi:10.1007/BF01081754.

Wright, I. C. (1994), Nature and tectonic setting of the southern Kermadec submarine arc volcanoes: An overview, *Mar. Geol.*, *118*, 217–236, doi:10.1016/0025-3227(94)90085-X.

Wright, I. C., W. Chadwick, C. E. J. de Ronde, D. Reymond, O. Hyvernaud, H. Gennerich, P. Stoffers, K. Mackay, M. Dunkin, and S. Bannister (2008), Collapse and reconstruction of Monowai submarine volcano, Kermadec arc, 1998–2004, *J. Geophys. Res.*, doi:10.1029/2007JB005138, in press.

Yoon, S. W., L. A. Crum, A. Prosperetti, and N. Q. Lu (1991), An investigation of the collective oscillations of a bubble cloud source, *J. Acoust. Soc. Am.*, *89*, 700–706, doi:10.1121/1.1894629.

Zimanowski, B., and R. Büttner (2003), Phreatomagmatic explosions in subaqueous volcanism, in *Explosive Subaqueous Volcanism*, *Geophys. Monogr. Ser.*, vol. 140, edited by J. D. L. White et al., pp. 51–60, AGU, Washington, D. C.

W. W. Chadwick Jr., R. P. Dziak, T. K. Lau, H. Matsumoto, and S. G. Merle, Hatfield Marine Science Center, Oregon State University, 2115 SE OSU Drive, Newport, OR 97365, USA. (bill.chadwick@noaa.gov)

K. V. Cashman and N. D. Deardorff, Department of Geological Sciences, University of Oregon, Eugene, OR 97403-1272, USA.

C. E. J. de Ronde, GNS Science, Ocean Exploration, P.O. Box 30368, Lower Hutt, 6315, New Zealand.

R. W. Embley, NOAA, Pacific Marine Environmental Laboratory, 2115 Oregon State University Drive, Newport, OR 97365-5258, USA.